On the Energetics of Quadrupedal Running: Predicting the Metabolic Cost of Transport via a Flexible-torso Model

Qu Cao and Ioannis Poulakakis

***Abstract*—In this paper, the effect of torso flexibility on the energetics of quadrupedal bounding is examined in a template setting. Two reductive sagittal-plane models, one with a rigid, non-deformable, torso and one with a flexible, unactuated, torso are proposed. Both models feature non-trivial leg mass and inertia to capture the energy associated with repositioning the legs after liftoff as well as the energy lost due to impacts. Bounding motions that minimize the cost of transport are generated for both models via a simple controller that coordinates leg recirculation. Comparisons reveal that torso compliance promotes locomotion efficiency by facilitating leg recirculation in anticipation to touchdown at speeds that are sufficiently high. Furthermore, by considering non-ideal torque generating and compliant elements with biologically reasonable efficiency values, it is shown that the flexible-torso model can predict the metabolic cost of transport for different animals, estimated using measurements of oxygen consumption. This way, the proposed model offers a means for approximating the energetic cost of transport of running quadrupeds in a simple and direct fashion.**

***Index Terms*—Quadrupedal bounding, energetics, templates, flexible torso, compliance.**

I. Introduction

Reductive mechanical models of legged locomotion – often termed "templates" (Full & Koditschek, 1999) – have long been employed to formally understand the mechanisms that support movement in legged animals and robots. The success of these models lies on their ability to predict fundamental locomotion properties, such as stability or maneuverability, without delving into the fine morphological characteristics of an animal or a robot.

Perhaps the most common reductive locomotion model is the Spring Loaded Inverted Pendulum (SLIP), introduced by Blickhan (1989) and McMahon and Cheng (1990) to study the biomechanics of running in humans and animals of different structure (Blickhan & Full, 1993; Full & Koditschek, 1999). Fundamentally, the SLIP explains how locomotion energy is distributed among its various forms; namely, kinetic, gravitational potential and elastic energy. However, due to its energy-conservative nature and its massless leg, the standard SLIP cannot capture the energy lost during locomotion as well as the energy required to recirculate the leg after liftoff in anticipation to touchdown. Thus, it cannot be used to assess the energetic cost of movement. With the purpose of evaluating energy consumption, a series of modified SLIP-like models have been proposed (Srinivasan & Ruina, 2005; Haberland et al., 2011; Srinivasan, 2011; Remy et al., 2012); these models incorporate different actuation schemes and dissipation sources, and can be used to study various hypotheses regarding the efficiency of legged locomotion.

Although non-conservative extensions of the standard SLIP have been useful in analyzing the energetic cost of transport (COT) – that is, the energy expenditure per unit weight and unit distance (Tucker, 1975) – of running, they cannot capture leg-torso coordination, which is an important determinant of the motion in quadrupedal gaits such as the bound or the gallop. On the other hand, models that address leg-torso coordination in quadrupedal running are either passive and conservative (Nanua, 1992; Poulakakis, 2002; Zhang et al., 2005; Poulakakis et al., 2006; Zou & Schmiedeler, 2006), or they concentrate primarily on controller design for specific quadrupedal robot platforms (Marhefka et al., 2003; Krasny & Orin, 2004; Culha & Saranli, 2011; Haueisen, 2011). The later typically employ computations of energy consumption in the form of suitable performance indices that are used to optimize running motions.

The aforementioned models – albeit useful for designing control laws for robotic quadrupeds – are not sufficient for explaining energy economy in quadrupedal *animal* running. This shortcoming is primarily due to the fact that none of these models – regardless of whether they include a rigid torso (Marhefka et al., 2003; Krasny & Orin, 2004), or an articulated torso (Culha & Saranli, 2011; Haueisen, 2011) – captures the effect of elastic energy storage elements located in the back of animals, such as muscle fibers, tendons and ligaments. Yet, as hypothesized by Alexander et al. (1985), the energy that is recycled through these elastic structures may significantly contribute to gait efficiency by promoting leg recirculation.

We hypothesize that the principal factors that determine the COT of running quadrupeds can be captured in a reduced-order model that incorporates torso compliance and springy legs with non-trivial mass. Along these lines, a sagittal-plane quadrupedal model with a segmented flexible torso is formulated in a non-dimensional setting. To provide insight on how torso flexibility affects energy economy, the proposed flexible-torso model is compared with a rigid-torso one in terms of COT computations. It is deduced that torso compliance enhances energy efficiency by facilitating leg recirculation, but only at velocities that are sufficiently high, thereby (conditionally) confirming the general hypothesis proposed by Alexander

Q. Cao and I. Poulakakis are with the Department of Mechanical Engineering, University of Delaware, Newark, DE 19716, USA; e-mail: {caoqu, poulakas}@udel.edu.

et al. (1985). In robot design, this observation implies that appropriately adjusted torso flexibility may improve efficiency in quadrupedal robots, provided that they are capable of realizing high performance running motions. Otherwise, the positive effect of torso compliance on energy efficiency may not be realized.

To assess the ability of the proposed flexible-torso model as a tool for predicting the metabolic COT of running quadrupedal animals, the model is extended to incorporate the energy lost due to non-ideal motor units and compliant elements. Despite the model's simple structure, and the fact that certain parameters are difficult to extract from available animal data, it is shown that the model-predicted COT matches exceptionally well the metabolic COT estimated using oxygen consumption measurements from running animals. Contrary to more morphologically complete models – as the one introduced by Herr and McMahon (2001), for example – the model proposed here does not explicitly rely on the fine details of an animal's structure and morphology. In that sense, it provides a relatively simple way to approximate the metabolic COT of quadrupedal animals with different sizes and structural characteristics.

Preliminary parts of this work have appeared previously in (Cao & Poulakakis, 2014); the present paper extends these results in two directions. First, it provides a more detailed discussion of the comparison between the rigid- and the flexible-torso models in terms of the mechanical COT. Second, it proposes a model-based way to estimate the metabolic COT of quadrupedal running, and it presents *direct* comparisons between the model-predicted metabolic COT with the one estimated by measurements of oxygen consumption of quadrupedal animals of different morphologies running at different speeds. To the best of the authors' knowledge, this is the first time that such direct comparison is undertaken in the context of a reduced-order model, demonstrating surprisingly good agreement with animal data.

The structure of the paper is as follows. Section II reviews related literature on the energetics of quadrupedal running. Section III describes, in a non-dimensional setting, two reductive quadrupedal models, one with and one without torso compliance. Section IV discusses the computation of cyclic bounding gaits in the context of the proposed models, and section V proposes two energy efficiency metrics – namely, the mechanical and the metabolic cost of transport – to assess the energy requirements of the computed motions. Section VI presents a comparison between the flexible- and rigid-torso models in the context of the mechanical cost of transport, and section VII demonstrates the ability of the flexible-torso model to predict the metabolic cost of transport of different quadrupedal animals. Finally, section VIII concludes the paper.

II. Background

Energy economy is important to both animals and robots. When covering long distances, it is hypothesized that animals tend to move in a manner that minimizes effort (Alexander, 1989). On the other hand, power-autonomous legged robots need to minimize energy consumption in order to maximize operation time (Seok et al., 2013). To quantify efficiency in legged locomotion the *cost of transport (COT)*[1] has been widely employed; the COT is a dimensionless quantity that measures the total energy required to move a unit weight over a unit distance (Tucker, 1975; Hoyt & Taylor, 1981; Collins et al., 2005).

Restricting our attention to quadrupedal running, only a limited number of models are capable of capturing gait energetics in a reductive setting. An early study was conducted by Nanua and Waldron (1995) in the context of an energy conservative, passive bounding model with massless legs. By assuming that the energy cost of running is proportional to the total kinetic energy, a performance index was formulated and minimized in order to compute cyclic bounding motions. However, this assumption – which was necessary given the conservative nature of the model – vastly simplifies the computation of the actual energy required to compensate for friction and impact losses as well as the energy needed to reposition the legs after liftoff (Schmiedeler et al., 2002). As a consequence, the motions computed based on the aforementioned model differ significantly from natural bounding gaits.

For similar reasons, a number of passive models of quadrupedal running that have appeared in the relevant literature – either with a rigid (Poulakakis, 2002; Zhang et al., 2005; Poulakakis et al., 2006; Zou & Schmiedeler, 2006) or an articulated (Seipel, 2011; Deng et al., 2012; Cao & Poulakakis, 2012; Yamasaki et al., 2013) torso – are fundamentally limited in their ability to predict the energy required to support motion.

More complete, non-conservative, quadrupedal running models that incorporate non-trivial leg mass have been proposed in the context of gait generation and control design (Marhefka et al., 2003; Krasny & Orin, 2004; Remy et al., 2010). To evaluate the performance of a fuzzy logic controller in generating efficient bounding and galloping motions, Marhefka et al. (2003) calculate the specific resistance including both positive and negative work and assuming ideal actuators. Aiming at optimizing running gaits, Krasny and Orin (2004) and more recently Remy et al. (2010) present computations of the COT taking into account only the positive work performed by ideal actuators. Partly because of this simplifying assumption, and partly because the metabolic COT of running animals encompasses a variety of internal phenomena that are difficult to model, the COT in Krasny and Orin (2004) differs significantly from the one generated from animal data in Hoyt and Taylor (1981). On the other hand, Remy et al. (2010) consider a quadrupedal model with series elastic actuators that apply inputs generated by Fourier series and compute running gaits that optimize a COT criterion; however, in the resulting gaits the legs undergo two retraction-protraction oscillations in a single stride, which is not common in animal and robot running.

All the non-conservative quadrupedal models mentioned thus far incorporate rigid non-deformable torsos. To assess the contribution of torso flexion-extension oscillations in the

[1] An alternative to the COT metric of energy expenditure in locomotion is the specific resistance introduced by Gabrielli and von Karman (1950) and used in (Poulakakis et al., 2005; Smith et al., 2010) to evaluate energy expenditure in robotic quadrupeds.

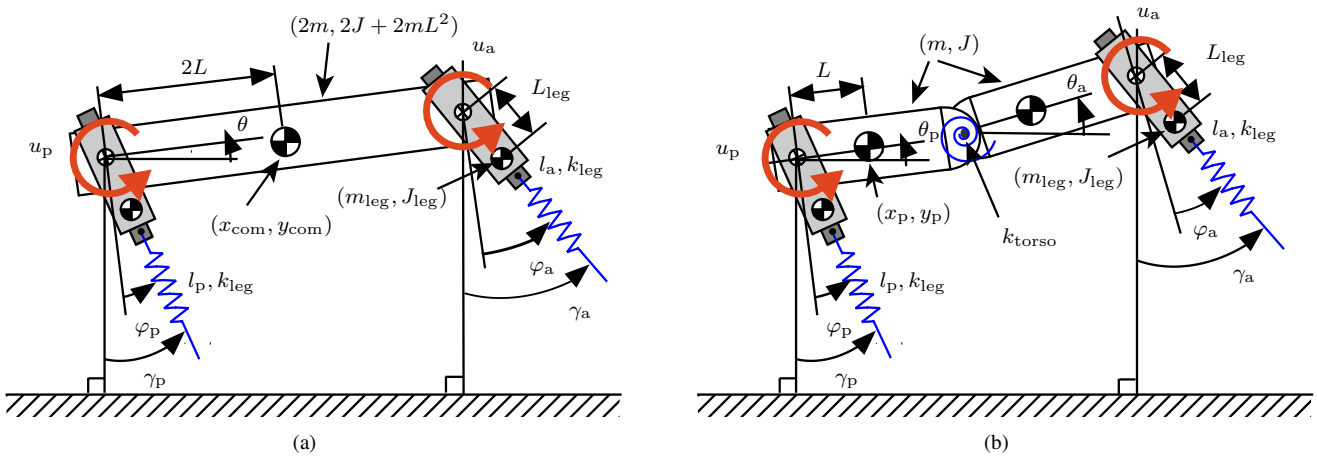

Fig. 1. Two sagittal-plane quadrupedal models used to study the energetics of bounding motion. (a) Rigid-torso model; (b) Flexible-torso model. The red arrows at the hip joints represent actuator inputs. In the flexible-torso model, the torso joint is not actuated.

generation of quadrupedal running gaits, Alexander (1988) proposed a model comprised of an articulated torso and massless legs. The model was then used to test the intuitive hypothesis put forward in earlier work of Alexander et al. (1985); namely, that elastic structures in animal's back promote energy economy by facilitating leg recirculation. However – due to the lack of compliant elements in the model – examination of the internal kinetic energy fluctuations associated with the torso movement lead to the conclusion that additional power will be required to maintain this motion, thereby not confirming the original hypothesis in Alexander et al. (1985). Recently, Culha and Saranli (2011) proposed a model that includes an articulated torso with an actuated spinal joint and springy legs with non-trivial mass. Optimization based on a modified version of the specific resistance that favors speed over efficiency resulted in bounding motions, which – in agreement with Alexander (1988) – require more energy compared to a rigid-torso model. Contrary to these findings, Haueisen (2011) deduced that an actuated torso can in fact improve gait efficiency, provided that high enough running speeds can be realized. This result though was obtained under the simplifying assumption that energy is supplied or lost only at discrete instants during the gait, while no comparisons with biological data was attempted.

Despite the many different models and the many different assumptions employed in evaluating the COT in quadrupedal running, the proposed approaches had limited success in producing results that are consistent with biological data. In part, this shortcoming may be attributed to the fact that none of the models discussed thus far – regardless of whether a rigid or an articulated torso is considered – incorporates torso flexibility. To the best of our knowledge, only Herr and McMahon (2001) consider the effect of torso flexibility in the context of galloping horse model. They report metabolic COT computations based on an empirical rule proposed by Kram and Taylor (1990), indicating good agreement with biological data of running horses extracted from the work of Hoyt and Taylor (1981). However, the model in (Herr & McMahon, 2001) is "animal specific," intended to capture the morphological characteristics of a horse, while manual tuning of the empirical rule by Kram and Taylor (1990) to estimate the metabolic energy was necessary to achieve agreement between simulation and experimental data.

With respect to (Herr & McMahon, 2001), the model proposed here is developed in a template setting – i.e., it is not grounded to the morphology of a specific animal or robot – thus, it is lower-dimensional and has the potential to capture gait energetics of running quadrupeds in a manner that is independent of specific morphological or structural details. As a result, it can offer a useful tool for evaluating the energy required to generate and sustain running motions in quadrupedal animals or robots, doing so in a direct manner, without relying on empirical formulas and data fitting.

III. Non-dimensional Reduced-order Models

To investigate the influence of torso compliance on the energetics of bounding, two sagittal-plane quadrupedal models with different torso configurations – one with a rigid non-deformable torso and one with a flexible segmented torso (Cao & Poulakakis, 2014) – are introduced; see figure 1. Both

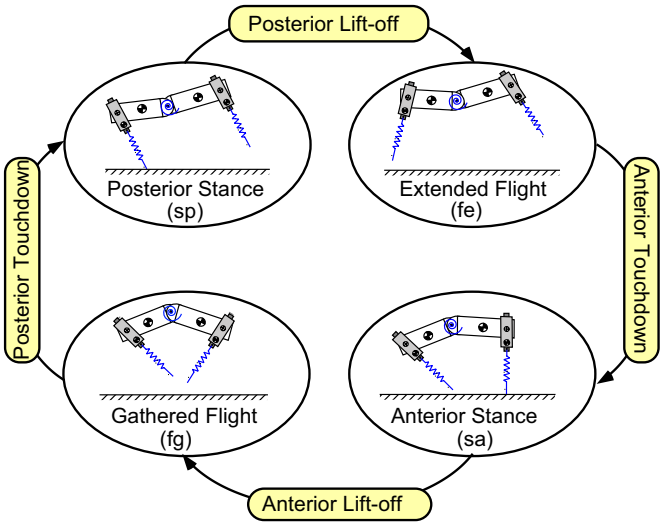

Fig. 2. Bounding phases and events.

models have the same leg structure: an upper segment with mass $m_{\rm leg}$ and moment of inertia $J_{\rm leg}$ about its center of mass (COM) and a lower segment represented by a massless prismatic spring of stiffness $k_{\rm leg}$. The natural length of the leg is denoted by l_0, corresponding to the distance between the hip and the toe when the leg spring is uncompressed. The distance between the COM of a leg and the corresponding hip joint is $L_{\rm leg}$. In both models, the interaction between the toe and the ground is modeled as an unactuated, frictionless pin joint.

The two models of figure 1 differ only in their torso structure. In the flexible-torso model of figure 1(b), the torso consists of two identical segments: the anterior and posterior parts with mass m, moment of inertia J about their COM and hip-to-COM spacing L. A rotational spring is inserted between the two segments to introduce flexibility, producing a torque

$$\tau_{\rm torso} = k_{\rm torso}\left[(\theta_{\rm a} - \theta_{\rm p}) - \theta_{\rm rest}\right] \ , \tag{1}$$

where $\theta_{\rm a}$, $\theta_{\rm p}$ are the pitch angles of the two segments as shown in figure 1(b), $\theta_{\rm rest} < 0$ is the rest angle of the spring and $k_{\rm torso}$ is its stiffness. For fair comparison, the torso mass, hip-to-COM distance and moment of inertia of the torso about the COM in the rigid-torso model are $2m$, $2L$ and $2J + 2mL^2$, respectively.

The bounding gait considered in this work is depicted in figure 2. Here, we only consider bounding without a double support phase. Depending on the state of the legs – whether on the ground or in the air – and the configuration of the torso of the flexible-torso model, the bounding cycle can be divided into four phases: the posterior stance phase, denoted by "sp," when only the posterior leg is on the ground; the anterior stance phase, denoted by "sa," in which only the anterior leg is in contact with the ground; the extended flight phase, denoted by "fe," when both legs are in the air and the torso exhibits a convex configuration; and, the gathered flight phase, denoted by "fg," when both legs are in the air and the torso assumes a concave configuration. The bounding gait considered for the rigid-torso model follows the same sequence as in figure 2, albeit there is no difference in the torso configuration between the gathered and extended flight phases. Both models exhibit continuous-time dynamics in each phase separated by event-triggered transitions.

A. Continuous-time dynamics in non-dimensional form

With reference to figure 1, in each stance phase $i \in \{\rm sp, sa\}$, the configuration space Q_i can be parameterized by the length of the leg in contact with the ground – that is, $l_{\rm p} \in \mathbb{R}$ for the posterior and $l_{\rm a} \in \mathbb{R}$ for the anterior stance phases – the leg angles $(\varphi_{\rm p}, \varphi_{\rm a}) \in \mathbb{S}^2$ relative to the torso, and the angles describing the configuration of the torso – namely, $(\theta_{\rm p}, \theta_{\rm a}) \in \mathbb{S}^2$ for the flexible-torso and θ for the rigid-torso model – i.e.[2],

$$q_i := \begin{cases} (l_{\rm p}, \varphi_{\rm p}, \varphi_{\rm a}, \theta_{\rm p}, \theta_{\rm a})' \in Q_i & \text{for} \quad i = \rm sp, \\ (l_{\rm a}, \varphi_{\rm p}, \varphi_{\rm a}, \theta_{\rm p}, \theta_{\rm a})' \in Q_i & \text{for} \quad i = \rm sa, \end{cases} \tag{2}$$

[2]Notation: To avoid cluttering, we denote the transpose of a vector x by x' instead of the commonly used symbol $x^{\rm T}$.

for the flexible-torso model, and

$$q_i := \begin{cases} (l_{\rm p}, \varphi_{\rm p}, \varphi_{\rm a}, \theta)' \in Q_i & \text{for} \quad i = \rm sp, \\ (l_{\rm a}, \varphi_{\rm p}, \varphi_{\rm a}, \theta)' \in Q_i & \text{for} \quad i = \rm sa, \end{cases} \tag{3}$$

for the rigid-torso model.

The flexible-torso model exhibits extended and gathered flight phases. In each of these phases, the configuration space Q_i, $i \in \{\rm fg, fe\}$, can be parameterized by the Cartesian coordinates $(x_{\rm p}, y_{\rm p}) \in \mathbb{R}^2$ of the COM of the posterior part of the torso, the pitch angles $(\theta_{\rm p}, \theta_{\rm a}) \in \mathbb{S}^2$ of the posterior and anterior parts of the torso, together with the angles $(\varphi_{\rm p}, \varphi_{\rm a}) \in \mathbb{S}^2$ of the legs relative to the torso; i.e,

$$q_i := (x_{\rm p}, y_{\rm p}, \varphi_{\rm p}, \varphi_{\rm a}, \theta_{\rm p}, \theta_{\rm a})' \in Q_i \quad \text{for} \quad i \in \{\rm fg, fe\} \ . \tag{4}$$

Similarly, the flight phases of the rigid-torso model can be parameterized by the Cartesian coordinates $(x_{\rm com}, y_{\rm com}) \in \mathbb{R}^2$ of the COM of the torso, its pitch angle $\theta \in \mathbb{S}^1$, and the angles $(\varphi_{\rm a}, \varphi_{\rm p}) \in \mathbb{S}^2$ of the legs with respect to the torso; i.e.,

$$q_i := (x_{\rm com}, y_{\rm com}, \varphi_{\rm p}, \varphi_{\rm a}, \theta)' \in Q_i \quad \text{for} \quad i \in \{\rm fg, fe\} \ . \tag{5}$$

The equations that govern the motion of both models in all phases can be derived using standard methods – as in (Spong et al., 2005, Chapter 7) for example – and can be brought in state-space form as

$$\begin{aligned} \dot{x}_i &= f_i(x_i) + g_i(x_i)u_i \\ &= f_i(x_i) + g_{i,\rm a}(x_i)u_{i,\rm a} + g_{i,\rm p}(x_i)u_{i,\rm p} \end{aligned} \tag{6}$$

where $x_i := (q_i', \ \dot{q}_i')'$ is the state vector for each phase $i \in \{\rm sp, sa, fg, fe\}$ evolving in $TQ_i := \{(q_i', \ \dot{q}_i')' |\ q_i \in Q_i, \dot{q}_i \in \mathbb{R}^{\dim(q_i)}\}$. The input $u_i := (u_{i,\rm p}, u_{i,\rm a})'$ includes the torques $u_{i,\rm p}$ and $u_{i,\rm a}$ applied at the posterior and anterior hip joints, respectively; see figure 1. Note that in both models, the hip torques are the only continuous-time inputs; the torso joint of the flexible-torso model in figure 1(b) is unactuated, and the torque developed between the posterior and anterior parts of the torso is solely due to the spring (1).

In (6), the physical properties of the each model are captured by the following parameters

$$\{m, m_{\rm leg}, J, J_{\rm leg}, l_0, L_{\rm leg}, L, k_{\rm torso}, k_{\rm leg}\} \ . \tag{7}$$

To reduce the number of parameters, the dynamics (6) can be transformed in a non-dimensional form by selecting the

TABLE I
NON-DIMENSIONAL PARAMETERS

Relative torso moment of inertia	$I := J/(mL^2)$
Relative leg mass	$M_{\rm leg} := m_{\rm leg}/m$
Relative leg moment of inertia	$I_{\rm leg} := J_{\rm leg}/(m_{\rm leg}l_0^2)$
Relative hip-to-torso COM distance	$d := L/l_0$
Relative hip-to-leg COM distance	$d_{\rm leg} := L_{\rm leg}/l_0$
Relative torso stiffness	$\kappa_{\rm torso} := k_{\rm tor}/(mgl_0)$
Relative leg stiffness	$\kappa_{\rm leg} := k_{\rm leg}l_0/(mg)$
Froude number	$Fr := \bar{v}/\sqrt{gl_0}$

characteristic time scale τ as

$$\tau := \sqrt{\frac{l_0}{g}} \ , \tag{8}$$

where g is the gravitational acceleration. Then, the configuration variables defined in (2)-(5) and their derivatives with respect to time obtain the non-dimensional form:

$$\zeta^* := \frac{\zeta}{l_0}, \quad \dot{\zeta}^* := \frac{\tau\dot{\zeta}}{l_0}, \quad \ddot{\zeta}^* := \frac{\tau^2\ddot{\zeta}}{l_0} \ , \tag{9}$$

for $\zeta \in \{x_{\rm p}, y_{\rm p}, x_{\rm com}, y_{\rm com}, l_{\rm p}, l_{\rm a}\}$ and

$$\psi^* := \psi, \quad \dot{\psi}^* := \tau\dot{\psi}, \quad \ddot{\psi}^* := \tau^2\ddot{\psi} \ , \tag{10}$$

for $\psi \in \{\varphi_{\rm p}, \varphi_{\rm a}, \theta_{\rm p}, \theta_{\rm a}, \theta\}$ where the superscript " * " denotes a dimensionless quantity. Based on these transformations, the non-dimensional input torque u_i^* is defined as:

$$u_i^* := \frac{u_i}{mgl_0} \ . \tag{11}$$

Substitution of (9) and (10) into (6) reduces the parameters in (7) to the following seven dimensionless quantities:

$$\{I, M_{\rm leg}, I_{\rm leg}, d, d_{\rm leg}, \kappa_{\rm torso}, \kappa_{\rm leg}\} \ , \tag{12}$$

the definitions of which are collected in table I for convenience. Finally, an additional dimensionless quantity provided in table I is the Froude number, Fr, which captures the average forward speed $\bar{v}$. It should be noted here that in some biological studies – as in (Alexander, 1989; Maes et al., 2008), for example – the Froude number is defined as $\bar{v}^2/(gl_0)$, which is the square of our definition.

B. Event-based transitions

The continuous-time phases are separated by the event-based transitions; namely, the touchdown and liftoff of the legs as in figure 2.

1) Flight-to-stance transitions: The flight phase terminates when the vertical distance between the toe of either the posterior or the anterior leg and the ground becomes zero. Due to the non-negligible mass of the upper leg, an impact occurs at touchdown. To avoid complexity, the impacts will be modeled as in (Westervelt et al., 2007, Section 3.4) under the following hypotheses:

- the toe colliding the ground neither rebounds nor slips;
- impacts are instantaneous;
- the actuator inputs can be ignored over an instantaneous impact;
- the forces applied by the ground during the impact can be represented by impulses;
- the impulsive forces result in instantaneous changes in velocities, but there is no instantaneous change in the configuration of the model.

Based on these assumptions, the flight phase dynamics can be integrated over the infinitesimally small duration of the impact to result in a linear map that is used to compute the states right after impact based on those right before.

2) Stance-to-flight transitions: In general, transitions from stance to flight occur when the vertical ground reaction force (GRF) becomes zero and the vertical acceleration of the toe is directed upwards. To simplify the analysis, we will assume that liftoff occurs when the leg spring extends to its natural length, i.e, $l_{\rm a}^*$ or $l_{\rm p}^* = 1$, as adopted in (Haberland et al., 2011).

IV. Generation of Efficient Bounding Motions

Our purpose in this work is to characterize the effect of torso flexibility on energy consumption and to assess the capacity of the flexible-torso model in predicting the energetic cost of transport in quadrupedal animal running. As a result, the objective of the controller used here to generate bounding is merely to recirculate the legs after liftoff and to replace the energy lost at impacts. No control action is developed for the leg that is in contact with the ground; the corresponding hip joint is *passive*, similarly to the passive bounding models studied in (Nanua & Waldron, 1995; Poulakakis et al., 2006; Deng et al., 2012; Cao & Poulakakis, 2012).

To make the comparison between the rigid-torso and the flexible-torso models as fair as possible, the proposed controllers will be developed using feedback linearization as in (Westervelt et al., 2007), and all the control parameters will be incorporated in the formulation of an optimization problem for computing running motions, thereby making their selection more systematic than manual gain tuning.

Note that the generated bounding motions are not necessarily stable, and further control action may be required in order to reject disturbances. Controllers that stabilize bounding motions can be found in (Cao & Poulakakis, 2013) and references therein. Recently, Cao and Poulakakis (2015) extended the controller in (Cao & Poulakakis, 2013) to a sagittal-plane model with nontrivial leg mass – similar to the one used here – and used this controller to realize speed transitions by switching among different bounding gaits using estimates of the domain of attraction obtained via sums-of-squares programming (Tedrake et al., 2010). Other recent methods include (Park & Kim, 2015), where galloping motions over a wide range of running speeds have been generated and stabilized by "shaping" the vertical ground reaction forces through the hip and knee torques of the (sufficiently actuated, non-compliant) leg in contact with the ground. Similarly to (Cao & Poulakakis, 2013, 2015), Park and Kim (2015) employed (virtual) holonomic constraints (Westervelt et al., 2007) to coordinate the swing motions of the anterior and the posterior legs based on the biological observation that the coupling of the hind- and fore-limbs determine the gait pattern (Miller et al., 1975).

Finally, to avoid cumbersome notation, hereafter we neglect " * " with the understanding that all the variables are the non-dimensional ones defined in (9), (10) and (11).

A. Leg recirculation control

As was mentioned above, the leg that is in contact with the ground is completely passive. Control action is developed only at the hip joint of the leg that is in flight, and the objective of the controller is to recirculate the leg in anticipation of

touchdown. In what follows, we describe the controller for the flexible-torso model; the corresponding controller for the rigid-torso model can be derived in an analogous fashion, and is omitted for brevity. Figure 3 summarizes the control inputs applied at the hip joints in each phase. Note that other control methods such as the PID controllers proposed by Culha and Saranli (2011) can also be used.

The design of the controller begins by associating a scalar output function of the form

$$y_i = h_i(q_i, \alpha_i) := q_{\mathrm{c},i} - h_i^{\mathrm{d}}(s_i(q_i), \alpha_i) \ , \tag{13}$$

to the dynamics (6) where $i \in \{\mathrm{sa}, \mathrm{fg}, \mathrm{sp}, \mathrm{fe}\}$. In (13), $q_{\mathrm{c},i}$ is the controlled variable and h_i^{d} represents its desired evolution that is parameterized via a set of parameters α_i as detailed below. The controlled variables are defined by

$$q_{\mathrm{c},i} := \begin{cases} \gamma_{\mathrm{p}} = \varphi_{\mathrm{p}} + \theta_{\mathrm{p}} & \text{for} \ \ i \in \{\mathrm{sa}, \mathrm{fe}\}, \\ \gamma_{\mathrm{a}} = \varphi_{\mathrm{a}} + \theta_{\mathrm{a}} & \text{for} \ \ i \in \{\mathrm{sp}, \mathrm{fg}\}. \end{cases} \tag{14}$$

In words, the controlled variable is selected to be

- the posterior absolute leg angle in the anterior stance and in the extended flight phases,
- the anterior absolute leg angle in the posterior stance and in the gathered flight phases.

1) Designing the constraints: In each phase $i \in \{\mathrm{sa}, \mathrm{fg}, \mathrm{sp}, \mathrm{fe}\}$, the desired evolution h_i^{d} in (13) is described via a 5-th order Beziér polynomial with coefficients $\alpha_i := \{\alpha_{i,k}\}_{k=0,\ldots,5}$; i.e.,

$$h_i^{\mathrm{d}}(s_i(q_i), \alpha_i) = \sum_{k=0}^{5} b_{i,k}(s_i(q_i))\alpha_{i,k} \ , \tag{15}$$

where the terms $b_{i,k}$ are given by

$$b_{i,k}(s_i) := \frac{5!}{k!(5-k)!} s_i^k (1 - s_i)^{5-k} \ , \tag{16}$$

in which the dependence on q_i has been suppressed, and s_i is the strictly monotonic quantity

$$s_i := \frac{\gamma^{\max} - \gamma}{\gamma^{\max} - \gamma^{\min}} \ . \tag{17}$$

In (17),

$$\gamma := \begin{cases} \gamma_{\mathrm{p}} & \text{for} \ \ i \in \{\mathrm{sp}, \mathrm{fg}\}, \\ \gamma_{\mathrm{a}} & \text{for} \ \ i \in \{\mathrm{sa}, \mathrm{fe}\}, \end{cases} \tag{18}$$

and $\gamma^{\max}$ and $\gamma^{\min}$ are the maximum and minimum values of γ in the corresponding phase.

To provide more intuition, (13)-(18) imply that, in each phase, the evolution of the absolute angle of one leg (depicted in black color in figure 3) is determined by that of the other leg, which is either passive (blue color in figure 3) or follows a retraction controller (red color in 3) as is detailed below. For example, in the stance-anterior phase, the controlled variable is the absolute angle γ_{p} of the posterior leg according to (14) and its desired evolution $h_{\mathrm{sa}}^{\mathrm{d}}$ is a function of the absolute angle γ_{a} of the anterior leg, as (17)-(18) imply. As a result, the output functions (13) depend only on the configuration variables q_i and the parameters α_i associated with the polynomials (15), and can therefore be interpreted as (virtual) holonomic constraints that coordinate the motion of the legs.

In what follows, we restrict our attention to bounding gaits in which the variable s_i defined by (17) is strictly monotonic with respect to time. This condition does not limit the motions that can be realized by the model, and it allows replacing time, effectively coordinating the motions of the legs with respect to an "internal" clock, as in (Westervelt et al., 2007). In the stance phases, the monotonicity of s_i for $i \in \{\mathrm{sa}, \mathrm{sp}\}$ implies that the stance leg is continuously swept backward, as is normally the case in natural bounding motions. During the flight phases, the monotonicity of s_i can be guaranteed through proper choice of the coefficients of the Beziér polynomials in (15), in conjunction with a swing-leg retraction controller[3], such as the one proposed in (Seyfarth, Geyer, & Herr, 2003).

To provide more details on ensuring the monotonicity of s_i, consider the gathered flight; i.e., s_{fg}. Prior to entering the gathered flight – that is, at the end of the anterior stance – known properties of the Beziér polynomials (Westervelt et al., 2007, Section 6.2) can be used to write the swing velocity of the posterior leg as

$$\dot{\gamma}_{\mathrm{p}} = 5(\alpha_{\mathrm{sa},5} - \alpha_{\mathrm{sa},4})\dot{s}_{\mathrm{sa}} \ . \tag{19}$$

Since s_{sa} is strictly monotonically increasing in stance anterior[4], i.e., $\dot{s}_{\mathrm{sa}} > 0$, choosing $\alpha_{\mathrm{sa},5} < \alpha_{\mathrm{sa},4}$ will force the posterior leg to swing backward (that is, $\dot{\gamma}_{\mathrm{p}} < 0$) at the beginning of the ensuing gathered flight phase. Choosing the input torque $u_{\mathrm{fg,p}}$ during the gathered flight according to the prescription

$$u_{\mathrm{fg,p}} = K_{\mathrm{p}} \dot{x}_{\mathrm{p}}^{\mathrm{toe}} \ , \tag{20}$$

where $K_{\mathrm{p}} < 0$ and $\dot{x}_{\mathrm{p}}^{\mathrm{toe}}$ is the forward velocity of the posterior toe relative to the ground allows us to make γ_{p} monotonically decreasing during the gathered flight. A similar procedure can be used to ensure the monotonicity of s_{fe} in the extended flight phase, resulting in introducing Beziér polynomial coefficients $\alpha_{\mathrm{sp},5} < \alpha_{\mathrm{sp},4}$ such that $\dot{\gamma}_{\mathrm{a}}$ is negative at the end of posterior stance phase, i.e,

$$\dot{\gamma}_{\mathrm{a}} = 5(\alpha_{\mathrm{sp},5} - \alpha_{\mathrm{sp},4})\dot{s}_{\mathrm{sp}} < 0 \ , \tag{21}$$

and a gain $K_{\mathrm{a}} < 0$ for the swing retraction controller, i.e.,

$$u_{\mathrm{fe,a}} = K_{\mathrm{a}} \dot{x}_{\mathrm{a}}^{\mathrm{toe}} \ . \tag{22}$$

Note that K_{p} and K_{a} are incorporated in the parameters that are used in the optimization problem of section V.

2) Imposing the constraints: To impose the constraints (13) on the dynamics (6) we differentiate (13) twice with respect to time to obtain

$$\begin{aligned} \frac{d^2 y_i}{d\tau^2} \ &= \ L_{f_i}^2 h_i(x_i, \alpha_i) + L_{g_{i,\mathrm{a}}} L_{f_i} h_i(q_i, \alpha_i) u_{i,\mathrm{a}} \\ &\quad + L_{g_{i,\mathrm{p}}} L_{f_i} h_i(q_i, \alpha_i) u_{i,\mathrm{p}} \ , \end{aligned} \tag{23}$$

[3]This controller has the additional advantage that it minimizes the horizontal speed of the toe relative to the ground at touchdown, thereby reducing the energy lost due to the impact and increasing the overall energy efficiency (Haberland et al., 2011).

[4]This is because the anterior leg is continuously swept backwards during the stance-anterior phase.

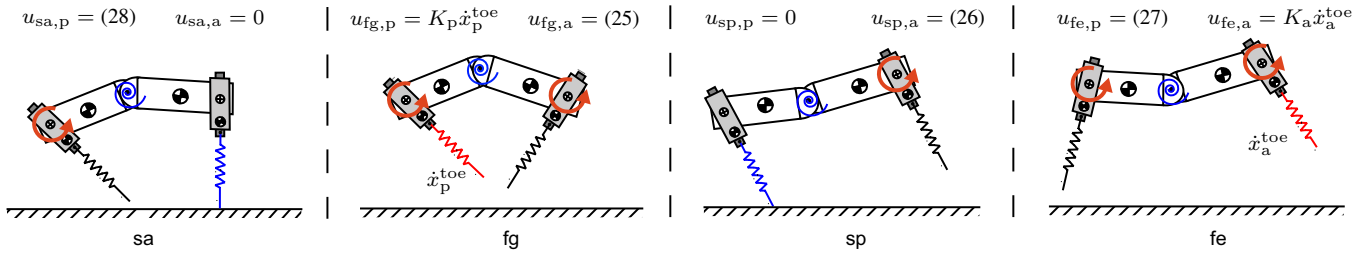

Fig. 3. Summary of the control actions in different phases. From left to right: anterior stance, gathered flight, posterior stance and extended flight. The arrows at the hip joints signify the application of torque and the blue, red and black colors of the leg springs correspond to the hip actuation patterns that are employed at different phases: (i) The blue color implies that the corresponding hip joint is passive. (ii) The red color means that a swing-leg retraction controller is applied at the corresponding hip joint. (iii) The black color indicates that the absolute leg angle of the corresponding leg is selected as the controlled variable, $q_{\mathrm{c},i}$, in (13) to enforce coordination between the motion of the legs.

where, in accordance with the notation in (Westervelt et al., 2007), $L^2_{f_i}h_i$, $L_{g_{i,\mathrm{a}}}L_{f_i}h_i$ and $L_{g_{i,\mathrm{p}}}L_{f_i}h_i$ are the Lie derivatives of the output function h_i defined by (13) along the vector fields f_i, $g_{i,\mathrm{a}}$ and $g_{i,\mathrm{p}}$ that participate in (6). Since in each phase one of the hip torques in u_i is either zero or determined by the swing-leg retraction controller (20) and (22), the other hip torque that participates in (23) can be determined so that

$$\frac{d^2 y_i}{d\tau^2} = 0 \ . \tag{24}$$

In more detail, in the gathered flight phase, the posterior torque $u_{\mathrm{fg,p}}$ is determined by (20). Then, provided that $L_{g_{\mathrm{fg,a}}}L_{f_{\mathrm{fg}}}h_{\mathrm{fg}}$ is invertible, the anterior hip input is given by

$$u_{\mathrm{fg,a}} = -(L_{g_{\mathrm{fg,a}}}L_{f_{\mathrm{fg}}}h_{\mathrm{fg}})^{-1}(L^2_{f_{\mathrm{fg}}}h_{\mathrm{fg}} + L_{g_{\mathrm{fg,p}}}L_{f_{\mathrm{fg}}}h_{\mathrm{fg}}u_{\mathrm{fg,p}}) \ . \tag{25}$$

In the ensuring posterior stance phase, since the posterior leg is kept passive and no hip torque is applied, the anterior hip input is simply

$$u_{\mathrm{sp,a}} = -(L_{g_{\mathrm{sp,a}}}L_{f_{\mathrm{sp}}}h_{\mathrm{sp}})^{-1}L^2_{f_{\mathrm{sp}}}h_{\mathrm{sp}} \ . \tag{26}$$

The input at the posterior joint in the extended flight and anterior flight phases can be derived in the same manner, resulting in

$$u_{\mathrm{fe,p}} = -(L_{g_{\mathrm{fe,p}}}L_{f_{\mathrm{fe}}}h_{\mathrm{fe}})^{-1}(L^2_{f_{\mathrm{fe}}}h_{\mathrm{fe}} + L_{g_{\mathrm{fe,a}}}L_{f_{\mathrm{fe}}}h_{\mathrm{fe}}u_{\mathrm{fe,a}}) \tag{27}$$

and

$$u_{\mathrm{sa,p}} = -(L_{g_{\mathrm{sa,p}}}L_{f_{\mathrm{sa}}}h_{\mathrm{sa}})^{-1}L^2_{f_{\mathrm{sa}}}h_{\mathrm{sa}} \ . \tag{28}$$

3) Closed-loop system: Figure 3 summarizes the control action that is applied at the hip joints of the model in each phase. The same control strategy is employed to recirculate the legs in the rigid-torso model; the legs are actuated only when they are in flight, and the hip torque of the leg providing support is equal to zero. With the inputs at the hip joints as in figure 3, the dynamics (6) in each phase can be written in closed-loop form as

$$\dot{x}_i = f_i^{\mathrm{cl}}(x_i, \alpha_i^{\mathrm{cl}}) \ . \tag{29}$$

where $\alpha_i^{\mathrm{cl}} = \alpha_i$ for $i \in \{\mathrm{sa}, \mathrm{sp}\}$, $\alpha_i^{\mathrm{cl}} = \{\alpha_i, K_{\mathrm{a}}, K_{\mathrm{p}}\}$ for $i \in \{\mathrm{fg}, \mathrm{fe}\}$, and α_i includes all the parameters associated with the output functions for each phase.

B. Poincaré return map

The dynamics of bounding can be described by concatenating the continuous-time phases according to the sequence of figure 2. To study the existence of such gaits, the method of Poincaré is used (Guckenheimer & Holmes, 1996). The Poincaré section is taken at liftoff of the anterior leg, i.e.,

$$\mathcal{S}_{\mathrm{sa}\to\mathrm{fg}} := \{x_{\mathrm{sa}} \in TQ_{\mathrm{sa}} \mid l_{\mathrm{a}} - 1 = 0, \ \dot{l}_{\mathrm{a}} > 0\} \ , \tag{30}$$

and the corresponding Poincaré return map $\mathcal{P} : \mathcal{S}_{\mathrm{sa}\to\mathrm{fg}} \to \mathcal{S}_{\mathrm{sa}\to\mathrm{fg}}$ is obtained by numerically integrating the closed-loop dynamics for each phase according to the phase sequence of figure 2. As a result,

$$x_{\mathrm{sa}}[k+1] = \mathcal{P}(x_{\mathrm{sa}}[k], \alpha^{\mathrm{cl}}) \ , \tag{31}$$

where $x_{\mathrm{sa}}[k]$ is the state at the end of the k-th anterior stance phase, and $\alpha^{\mathrm{cl}} = \{\alpha^{\mathrm{cl}}_{\mathrm{sa}}, \alpha^{\mathrm{cl}}_{\mathrm{fg}}, \alpha^{\mathrm{cl}}_{\mathrm{sp}}, \alpha^{\mathrm{cl}}_{\mathrm{fe}}\}$ includes the parameters introduced by the continuous-time controllers of Section IV-A. Then, the problem of computing periodic bounding gaits becomes equivalent to finding a state vector x_{sa} so that

$$x_{\mathrm{sa}} - \mathcal{P}(x_{\mathrm{sa}}, \alpha^{\mathrm{cl}}) = 0 \tag{32}$$

for suitable parameter values α^{cl}.

V. Methods: Searching for Fixed Points

As a measure of the energy required to generate cyclic bounding motions in the two models of figure 1, we use the *cost of transport (COT)*, a dimensionless quantity defined as the energy consumed over a distance divided by that distance and the weight of the system (Tucker, 1975). In this work, we use two variations of the COT depending on whether the energy dissipated within the motor units and the springs is considered.

A. Mechanical cost of transport

The mechanical COT, c_{mc}, characterizes the power delivered at the joints of the system, and is computed by

$$c_{\mathrm{mc}} = \frac{1}{2(1+M_{\mathrm{leg}})TFr}\int_0^T (|u_{\mathrm{a}}\dot{\varphi}_{\mathrm{a}}| + |u_{\mathrm{p}}\dot{\varphi}_{\mathrm{p}}|)d\tau \ , \tag{33}$$

where T is the non-dimensional stride period and the rest of the variables have been defined in section III-A. The mechanical COT (33) is useful in comparing the rigid- and flexible-torso models of figure 1 from an "output" perspective – that is, from the point of view of the mechanics of the

generated motion. Such comparison can determine the effect of various model parameters – including torso compliance – on the energetics of bounding, without relying on the specific characteristics of the actuators – motors or muscles – that are used to deliver the required power to the system's joints.

B. Metabolic cost of transport

To assess the capacity of the proposed models to capture energy consumption in animal running, the definition of the COT needs to be extended so that it incorporates the efficiency of the motor units and the compliant members in injecting and recycling the energy required to sustain the motion. This is necessary because the mechanical COT is difficult to compute based on experimental data from animal running (Alexander, 2005). Instead, it is more convenient to measure oxygen consumption in experiments with running animals, from which the metabolic COT can be obtained; see section VII-A below for more details.

To capture the metabolic COT in animal running, we modify (33) in two ways. First, the efficiency of the motor units in performing positive and negative work is taken into account, so that the power required at the hip joints is computed as

$$P_1 = \frac{1}{\eta_1}([u_{\rm a}\dot{\varphi}_{\rm a}]^+ + [u_{\rm p}\dot{\varphi}_{\rm p}]^+) + \frac{1}{\eta_2}([u_{\rm a}\dot{\varphi}_{\rm a}]^- + [u_{\rm p}\dot{\varphi}_{\rm p}]^-) \ , \tag{34}$$

where

$$[P]^+ = \begin{cases} P & \text{if } P \geq 0, \\ 0 & \text{if } P < 0, \end{cases} \quad \text{and} \quad [P]^- = \begin{cases} 0 & \text{if } P \geq 0, \\ -P & \text{if } P < 0, \end{cases}$$

and η_1 and η_2 are the corresponding efficiencies. The definition of P_1 is based on the assumption that the metabolic energy consumed by muscles is roughly proportional to the mechanical power they generate, albeit with different efficiencies for positive and negative work (Margaria, 1976). Following Margaria (1976), the coefficients η_1 and η_2 are then set as

$$\eta_1 = 0.25 \ \text{ and } \ \eta_2 = 1.2 \ ,$$

where $\eta_2 > 1$ reflects the fact that muscles recycle part of the energy when doing negative work.

The second modification to (33) is modeling the leg and torso compliance via non-ideal springs that dissipate part of the mechanical energy as they deform during leg compression and decompression and torso flexion and extension. Following Haberland et al. (2011), we will assume that the mechanical power dissipated in non-ideal springs is proportional to the power recycled by ideal springs so that

$$P_2 = \eta_3 \ \kappa_{\rm leg}(|(1-l_{\rm a})\dot{l}_{\rm a}| + |(1-l_{\rm p})\dot{l}_{\rm p}|)$$
$$P_3 = \eta_3 \ \kappa_{\rm torso}|(\theta_{\rm a}-\theta_{\rm p}-\theta_{\rm rest})(\dot{\theta}_{\rm a}-\dot{\theta}_{\rm p})| \ ,$$

where η_3 is a coefficient, which, based on physiological data regarding tendon efficiency provided by Pollock and Shadwick (1994), is selected as

$$\eta_3 = 0.1 \ .$$

It should be emphasized that η_1, η_2 and η_3 are *not* free parameters chosen by an optimization algorithm to achieve the best fit between simulation and experimental data from animal running. Instead, these coefficients are kept *constant* and equal to the biologically plausible values provided above, representing the efficiency of muscles when performing positive and negative work, and the efficiency of tendons in recycling mechanical energy. With these modifications to (33), the metabolic COT can be estimated by

$$c_{\rm mt} = \frac{1}{2(1+M_{\rm leg})TFr}\int_0^T (P_1+P_2+P_3)d\tau \ . \tag{35}$$

C. Optimization

With the mechanical and metabolic COT defined by (33) and (35), respectively, the search for efficient bounding motions can be cast as a constrained optimization problem, in which the task is to find fixed points to (32) that minimize the corresponding COT; i.e.,

$$\begin{aligned} \mathbf{min}\big\{c_{\rm mc}(x_{\rm sa},\alpha^{\rm cl}) \ \text{ or } \ c_{\rm mt}(x_{\rm sa},\alpha^{\rm cl})\big\} \\ \text{such that} \quad x_{\rm sa} = \mathcal{P}(x_{\rm sa},\alpha^{\rm cl}). \end{aligned} \tag{36}$$

This problem is solved using MATLAB's `fmincon`.

Although the existence of local minima cannot be precluded, once a fixed point is found for a specific speed, we continue searching for a better solution by using the current one as the initial guess and adding the constraint that the COT of the new fixed point should be smaller than the current value. The optimization terminates when this iterative algorithm cannot further improve the solution.

VI. Results: Mechanical COT

In this section, the effect of torso compliance on the mechanical COT of bounding will be discussed in the context of the two models introduced in section III. Through detailed parametric studies, the main factors that affect the mechanical COT of the system are investigated and conclusions that are helpful in designing efficient quadrupedal robots with torso compliance are drawn.

A. Comparison of the mechanical COT

Using the optimization framework described in section IV, the mechanical COT of bounding gaits that are realized in both the rigid and flexible torso models can be compared for different speeds and physical parameters.

We begin our discussion with figure 4, which shows the mechanical COT computed for different dimensionless hip-to-COM distances $d \in \{0.34, 0.38, 0.42\}$ and for various traveling velocities, as these are captured by the Froude number $Fr \in [1.5, 5.0]$, which roughly describes the running speed range of most animals (Alexander, 1989). In interpreting these results, note that $d := L/l_0$, so that a large value of d corresponds to a longer torso relative to the leg length. The rest of the parameters are kept constant and are given in table II. It should be mentioned that all the bounding motions computed based on the flexible-torso model and depicted in figure 4 exhibit pronounced torso oscillations.

It is clear from figure 4 that the energy consumption increases with the traveling speed in both models. Furthermore,

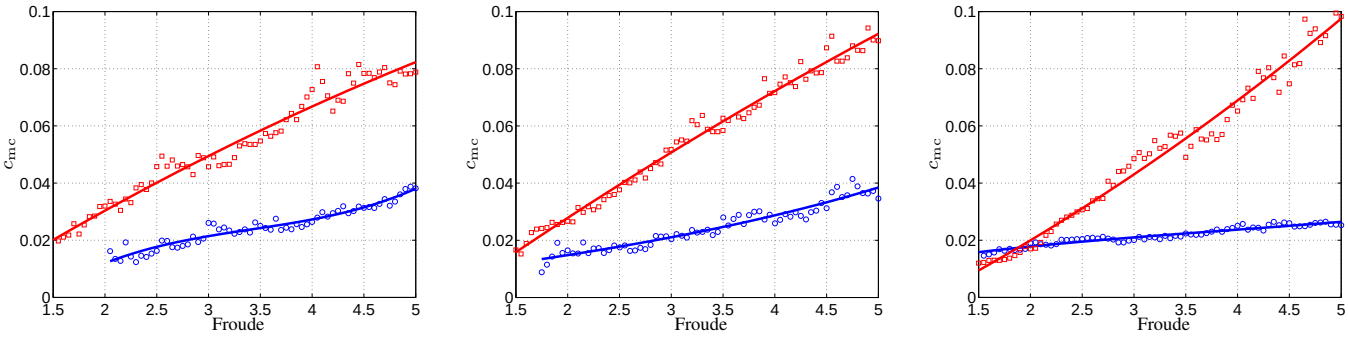

(a) $d = 0.34$ (b) $d = 0.38$ (c) $d = 0.42$

Fig. 4. The mechanical COT of flexible-torso (blue circles) and rigid-torso (red squares) models of different speeds and relative hip-to-COM distances. The continuous lines are fitted third degree polynomials.

there exists a threshold value for the Froude number, below which it was either impossible to compute fixed points in the flexible-torso model, as in figure 4(a) and 4(b), or the fixed points resulted in relatively higher mechanical COT than those of the rigid-torso model, as in figure 4(c). This observation implies that the benefits of torso flexibility in terms of energy efficiency are most appreciated at higher traveling speeds. This is evident from figure 4, where it is seen that the difference between the mechanical COT for the flexible- and rigid-torso models is amplified at higher Froude numbers.

Finally, figure 4(c) shows that the threshold value for the Froude number beyond which the flexible-torso model becomes more efficient is approximately equal to 1.8. It is interesting to note that this value corresponds to the transition from trotting to galloping, which is the same in animals with drastically different geometries (Alexander, 1989), such as horses and dogs (Hoyt & Taylor, 1981; Maes et al., 2008).

TABLE II
NON-DIMENSIONAL MECHANICAL PARAMETERS OF THE MODELS

Parameters	I	M_{leg}	I_{leg}	d_{leg}	κ_{leg}	κ_{tor}	θ_{rest}
Values	1.8	0.1	0.01	0.25	25.8	5.5	-0.17

B. *Torso oscillation and energy efficiency*

The models of section III effectively capture the energetic cost of recirculating the legs in flight, and thus allow the assessment of the contribution of the flexible torso to the efficiency of the gait. In fact, the improved efficiency of the flexible-torso model observed in figure 4 can be attributed to the torso's dorsoventral oscillations: as the torso flexes it facilitates the motion of the anterior leg backward and of the posterior leg forward, and vice versa when the torso extends.

In more detail, figure 5 shows the evolution of the absolute and relative leg angles for one of the fixed points of figure 4(c); namely, the fixed point corresponding to $d = 0.42$ and $Fr = 3.0$. It can be seen from figure 5 that, for the rigid-torso model, the evolution of the absolute angle of the posterior, γ_{p}, and anterior, γ_{a}, legs does not differ significantly from that of the corresponding relative angles φ_{p} and φ_{a}. By way of contrast,

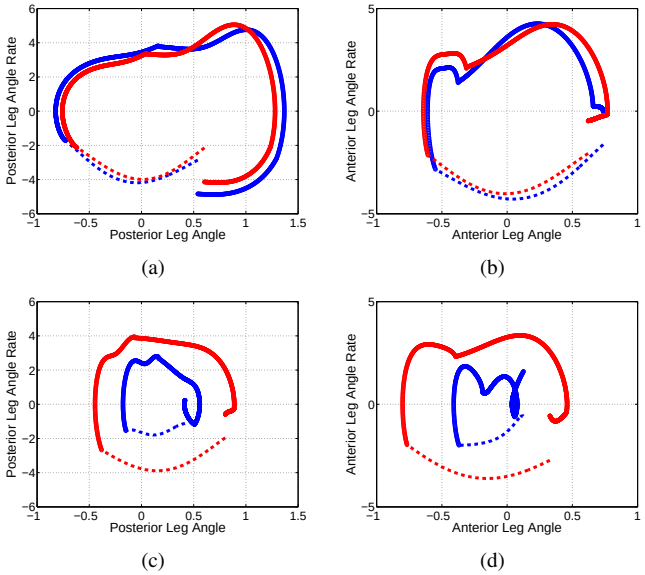

(a) (b) (c) (d)

Fig. 5. Absolute (red) and relative (blue) leg angles for a bounding gait at $Fr = 3.0$ with $d = 0.42$ for rigid-torso (a, b), and flexible-torso (c, d) models. The dotted line represent the stance phase. The discontinuity in leg angle rate is due to the impacts at touchdown.

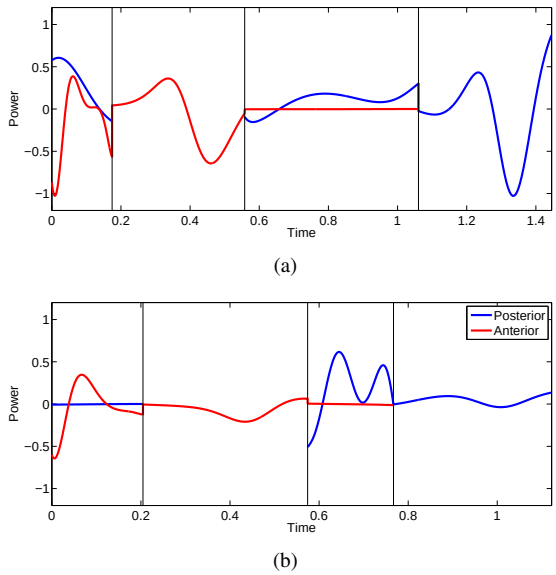

(a) (b)

Fig. 6. Power of the posterior (blue) and anterior actuators (red) in one stride of the rigid-torso model (a) and the flexible-torso model (b). The vertical lines separate the four phases; from left to right: flight-gathered (fg), stance-posterior (sp), flight-extended (fe), and stance-anterior (sa).

the differences between $\gamma_{\rm p}$ and $\varphi_{\rm p}$, and $\gamma_{\rm a}$ and $\varphi_{\rm a}$ are much larger in the flexible-torso model[5].

Unlike the pitch motion of the rigid-torso model – which shows little effect on leg recirculation – the torso's oscillation in the flexible-torso model significantly contributes to repositioning the leg during flight. Note though that as the value of the Froude number decreases, the difference between γ and φ in the flexible-torso model becomes smaller due to the decreased amplitude of the torso oscillation, the contribution of which to energy efficiency is reduced until it diminishes for $Fr < 1.8$. Figure 6 shows the input power during one stride of the fixed points depicted in figure 5. During the stance[6] phases "sa" and "sp", figures 6(a) and 6(b) show that the hip power required to place the corresponding swing leg forward in anticipation of touchdown is much smaller when torso flexibility is present indicating that it acts as an effective energy-saving mechanism.

Finally, figure 7 shows the stride frequency and length of the bounding motions presented in figure 4. It can be seen that as the forward speed increases, the stride frequency of the flexible-torso model remains almost constant. Correspondingly, a linear increasing relationship exist between the forward speed and the stride length for the flexible-torso model. This observation is consistent with biological data in (Hildebrand, 1961; Maes et al., 2008) showing that, at high-speed running gaits, quadrupedal mammals increase their velocity by increasing stride length instead of stride frequency.

[5]Note that the relative and absolute leg angles of fixed points of the flexible-torso model shown in figure 4(c) corresponding to $Fr > 1.8$ present similar behavior to that in figure 5.

[6]It is reminded that during the stance phase no torque is applied at the hip joint of the leg providing support.

C. Other parameters

1) Torso stiffness: In previous work, it was shown that the stiffness of the torso spring has a significant effect on both motion generation and gait stability (Cao & Poulakakis, 2013); here, we investigate its relationship with gait efficiency as shown in figure 8(a). For low stiffness, the mechanical COT increases linearly as the Froude number increases. However, for stiffer torso springs, the linear relationship between the mechanical COT and the Froude number becomes parabolic. This implies that when the torso stiffness is high enough, there is an optimal velocity that results in minimum energy consumption. Note that this parabolic dependence resembles the COT of galloping horse in (Hoyt & Taylor, 1981; Minetti et al., 1999). Furthermore, it is interesting to note that within the parabolic dependency region ($\kappa_{\rm torso} > 5.5$), the mechanical COT achieves its minima at a specific Froude number (≈ 3.0), which is independent of the value of the torso stiffness as indicated by figure 8(a).

Finally, figure 8(b) shows the *dimensionless* stride frequency of the fixed points in figure 8(a). It can be seen that, for the same *relative* torso stiffness, $\kappa_{\rm tor}$, the dimensionless stride frequency is almost constant over a range of values of the Froude number, as was seen in figures 7(a)–7(c). Furthermore, as the relative torso stiffness increases, the nearly constant relationship between the stride frequency and the Froude number shifts to higher frequency values.

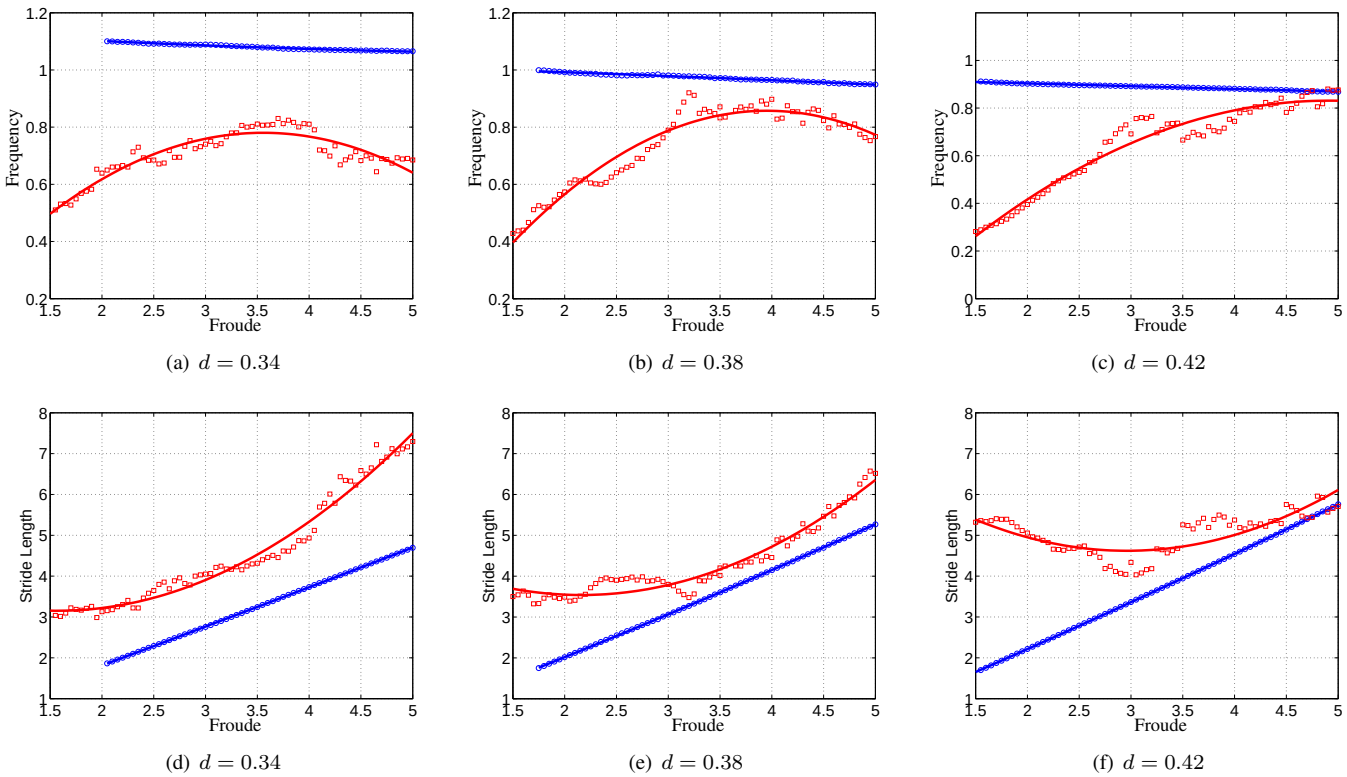

(a) $d = 0.34$ (b) $d = 0.38$ (c) $d = 0.42$

(d) $d = 0.34$ (e) $d = 0.38$ (f) $d = 0.42$

Fig. 7. The stride frequency (a, b, c) and stride length (d, e, d) of flexible-torso (blue circles) and rigid-torso (red circles) models at different speed and relative hip-to-COM distance. The continuous lines are fitted 3rd-order polynomials.

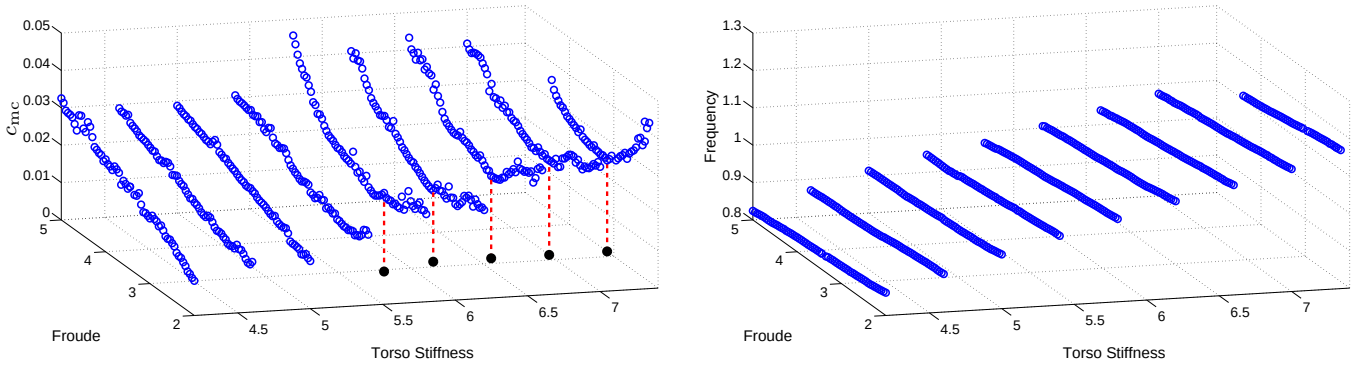

(a) (b)

Fig. 8. (a) The relationship between the torso stiffness and the mechanical COT at different speeds. The black dots are the projections of the points with minimal mechanical COT. (b) The relationship between the torso stiffness and the stride frequency at different speeds.

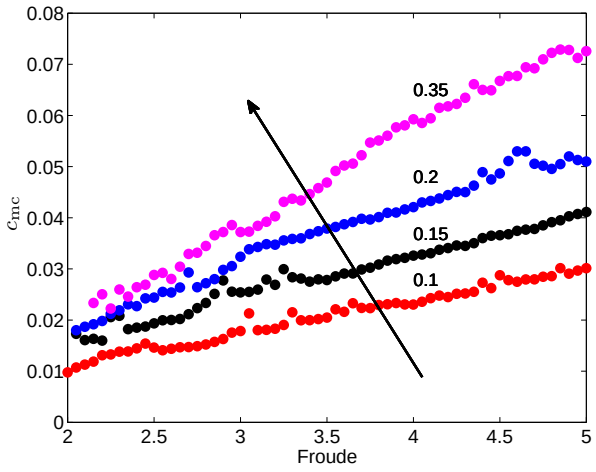

Fig. 9. COT of the flexible-torso model with relative leg mass $M_{\text{leg}} \in \{0.1, 0.15, 0.2, 0.35\}$, $d = 0.38$ and $k_{\text{torso}} = 5.5$. Note that $M_{\text{leg}} := m_{\text{leg}}/m$.

2) Leg mass: Another factor significantly affecting the mechanical COT is the mass of the leg. Larger mass requires larger torque to recirculate the leg, and it also results in larger energy dissipation at impacts (Ananthanarayanan, Azadi, & Kim, 2012; Seok et al., 2013). As expected, figure 9 shows that the mechanical COT of the flexible-torso model increases with the leg mass. Furthermore, increasing the mass of the leg appears to have a larger effect at higher speeds, suggesting that light leg design is critical for quadrupedal robots that are intended to realize high-performance, efficient running motions (Ananthanarayanan et al., 2012; Seok et al., 2013).

VII. Results: Metabolic COT

In previous sections, the influence of certain model parameters on the energetics of bounding with and without torso flexibility has been examined in the context of the mechanical COT. In this section, we turn our attention to assessing the ability of the proposed models to capture the energetics of quadrupedal *animal* running. In particular, the usefulness of the flexible-torso and the rigid-torso models as predictive tools for computing the efficiency of fast running motions of quadrupedal animals of different morphological characteristics is investigated. Most important, it is deduced that the flexible-torso model, suitably adapted to the geometric and morphological characteristics of different quadrupedal animals, can capture their metabolic COT, as this is estimated based on experimental data.

A. Animal data and computations

In our analysis, four animal species – namely, the horse (*Equus caballus*), the cheetah (*Acinonyx jubatus*), the gazelle (*Gazella gazella*) and the dog (*Canis familiaris*) – are considered, primarily due to the availability of data of oxygen consumption while running at high speeds.

1) Metabolic COT and Froude number: In general, the mechanical COT is difficult to obtain using animal data (Alexander, 2005); instead, the metabolic COT is more easily accessible on the basis of measurements of oxygen consumption. In more detail, the metabolic COT of animal running is computed from data on the mass-specific rate of oxygen consumption given the energy produced by a unit volume of oxygen and the corresponding running speed as, in (Minetti et al., 1999); i.e,

$$c_{mt} = \frac{V_{\text{O}_2} E_{\text{O}_2}}{mg\bar{v}} \quad , \tag{37}$$

where $V_{\text{O}_2}(\text{ml/s})$ is the rate of oxygen consumption, m (kg) is the mass of the animal, $g(\text{m/s}^2)$ is the gravitational acceleration and $\bar{v}(\text{m/s})$ is the average running speed. The energy produced per unit volume of oxygen consumed, E_{O_2}, is taken equal to 20.1J/ml according to Heglund and Taylor (1988) and Minetti et al. (1999).

The oxygen consumption rate of the horse is taken from Eaton et al. (1995) with running speeds in the range $\{7, 8, 9, 10, 11, 12, 13\}\text{m/s}$. The Froude number corresponding to each speed is computed under the assumption that the leg length is 1.3m, the same as the Dutch Warmblood horse with a similar weight (500kg) (Buchner et al., 1997). The metabolic COT of the dog is obtained from Kram and Taylor (1990), where data from running at $\{5, 6, 7\}\text{m/s}$ are provided. The leg length is set at 0.5m based on the morphological measurements of a dog with similar weight (25kg)

TABLE III
NON-DIMENSIONAL PHYSICAL PARAMETERS OF CERTAIN ANIMALS

Species	I	d	$M_{\rm leg}$	$I_{\rm leg}$	$d_{\rm leg}$	$\kappa_{\rm leg}$	$\kappa_{\rm tor}$
Horse	**1.2**	**0.34**	**0.24**	**0.03**	**0.30**	**28**	[4.0, 7.0]
Dog	**1.1**	**0.36**	**0.21**	**0.06**	**0.32**	**22**	[4.0, 7.0]
Cheetah	[0.9, 1.3]	**0.36**	**0.40**	[0.02, 0.08]	**0.25**	[20, 30]	[4.0, 7.0]
Gazelle	[0.9, 1.3]	**0.36**	**0.31**	[0.02, 0.08]	**0.03**	[20, 30]	[4.0, 7.0]

in (Farley et al., 1993). Finally, the oxygen consumption rate of the cheetah and the gazelle are obtained from Taylor et al. (1974), at speeds $\{4.75, 5.52\}\mathrm{m/s}$ for the cheetah and $\{5.02, 5.28, 5.71, 6.13\}\mathrm{m/s}$ for the gazelle. The corresponding leg lengths are obtained from the same paper. Note that for all the animals, only the metabolic data at high running speeds ($Fr > 1.8$) are included for comparison with the model prediction.

2) Non-dimensional model parameters: For a fair comparison between the model-predicted metabolic COT and the one estimated from biological data (37), the non-dimensional parameters that participate in the definition of the models, and are listed in table I, must be computed using the corresponding inertia, geometric and stiffness properties of the animals for which metabolic data are available. Clearly, it is difficult – if not impossible – to obtain measurements of all the required animal properties from the relevant literature. Yet, some non-dimensional parameters can be computed directly based on animal data; these parameters are given in bold in table III. Other parameters – such as the relative torso stiffness $\kappa_{\rm tor}$, for example – are not accessible from animal data. For these parameters, a range of values is examined when computing the model-predicted metabolic COT as is described below.

In more detail, all the geometric and inertia[7] properties of the horse are calculated from anatomic data that are available for the Dutch Warmblood horse (Buchner et al., 1997). The corresponding leg stiffness is adopted from Herr et al. (2002). For the dog, the torso mass, length and moment of inertia are taken from Schmiedeler et al. (2002) and Schmiedeler and Funke (2013) and the leg stiffness is obtained from Farley et al. (1993). The COM position of the leg and the leg mass are based on data from magnetic resonance image analysis provided in (Amit et al., 2009). Finally, for the cheetah and the gazelle, the torso mass, leg length, leg mass and the COM position of the leg are taken from Taylor et al. (1974), resulting in the values of $\{d, M_{\rm leg}, d_{\rm leg}\}$ that are given in table III.

As was mentioned above, not all the required model parameters are accessible from animal data published in the relevant literature. Thus, a range of possible values for these unknown parameters is considered. One such parameter is the relative torso stiffness $\kappa_{\rm tor}$, which in all the four species is assumed to take values in the range $[4.0, 7.0]$. Furthermore, for the cheetah and the gazelle, it was not possible to extract values for the relative moment of inertia of the torso segments and the leg as well as the relative stiffness of the leg. For these animals, the range of values for I and $I_{\rm leg}$ were chosen as $[0.9, 1.3]$ and $[0.02, 0.08]$ respectively to include the corresponding values of the horse and the dog; see table III. The range of $\kappa_{\rm leg}$ was selected as $[20, 30]$ capturing the leg stiffness values of many quadrupedal animals (Farley et al., 1993). It is important to mention that in computing the metabolic COT, the overall range of values of the parameters $\{I, I_{\rm leg}, \kappa_{\rm leg}, \kappa_{\rm torso}\}$ is discretized and all possible combinations of values are considered, as is detailed in the following section.

3) Computations: With the parameter values of table III, both the flexible- and the rigid-torso models are particularized to the morphology of each of the animals in consideration, for which measurements of oxygen consumption are available. The resulting models are then used to compute energy-efficient bounding motions that minimize the metabolic COT defined by (35) according to the procedure outlined in section V. The results are shown in figure 10, which – at different values of the Froude number – presents the metabolic COT predicted based on the flexible-torso (figure 10(a)) and on the rigid-torso (figure 10(b)) models together with the one obtained by (37) using measurements of oxygen consumption found in the relevant literature.

In interpreting figure 10 note that for each of the animals considered, and at each value of the Froude number, a collection of values of the (minimum) model-predicted metabolic COT is computed; each of these values corresponds to a different combination of model parameters $I, I_{\rm leg}$, $\kappa_{\rm leg}$ and $\kappa_{\rm tor}$, in the ranges given in table III. To ease computations, the ranges of the parameters are discretized as $\{0.9, 1.1, 1.3\}$ for I, $\{0.02, 0.04, 0.06, 0.08\}$ for $I_{\rm leg}$, $\{20, 25, 30\}$ for $\kappa_{\rm leg}$, and $\{4.0, 5.0, 6.0, 7.0\}$ for $\kappa_{\rm tor}$. Note that not all the combinations of these discrete parameter values result in cyclic bounding motions; hence, figure 10 presents the average value and the corresponding standard deviation of the (minimum) metabolic COT corresponding to all the combinations of parameters for which bounding motions can be generated.

B. Discussion

The main conclusion from figure 10 is that the metabolic COT predicted by the flexible-torso model is in striking agreement – given the simplicity of the model as well as the inaccuracy of the parameter values – with the one computed using measurements of oxygen consumption from experiments with running animals. The largest deviation is observed in the

[7]Note that the moment of inertia J of half the torso is required in order to compute the dimensionless moment of inertia I; see table I for the definition of I. However, J is not directly available from animal data; yet, the moment of inertia of the whole torso can be found in the relevant literature. Then, a reasonable approximation of J can be obtained given the torso mass m and the torso length L by assuming the moment of inertia of the whole torso is $2J + 2mL^2$ and solving for J as mentioned in section III.

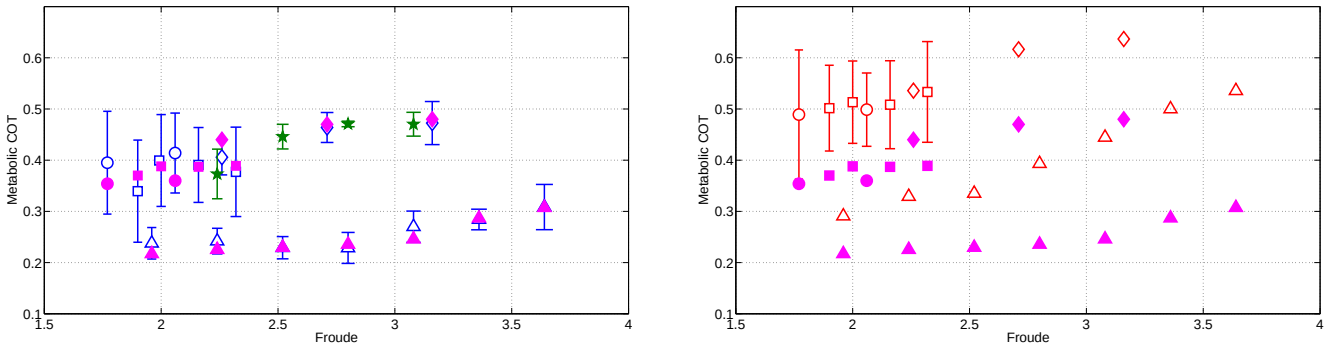

Fig. 10. The metabolic COT computed by (37) using oxygen consumption measurements (magenta filled symbols in both figures) and the corresponding model-predicted values at different running speeds. (a) Flexible-torso model (blue open symbols); (b) Rigid-torso model (red open symbols). Four animal species are considered in the analysis; cheetah (circles), dog (diamonds), horse (triangles) and gazelle (squares). The metabolic COT values for the "test" model are represented by green stars. In both figures, the error bars signify the standard variation of the model-predicted data due to the range of the parameter values considered in the corresponding computations.

gazelle and the cheetah, and is attributed to the fact that, for these two cases, only three out of the seven physical parameters required by the model are available based on direct morphological measurements; for the rest of the parameters, a range of possible values is considered, as shown in table III. On the other hand, the metabolic COT predicted by the rigid-torso model is consistently *larger* than the one estimated using animal data. Particularly for the dog and the horse where animal data at larger values of the Froude number are available, the discrepancy between the rigid-torso model prediction of the metabolic COT and the one computed by animal data becomes more pronounced.

To further explore the differences between the flexible- and the rigid-torso models in predicting the metabolic COT, figure 11 provides information regarding the stride length and the non-dimensional stride frequency of the computed optimal motions and compares them with animal values for the cases of the dog and the horse, for which the corresponding data are available in (Maes et al., 2008) and in (Eaton et al., 1995), respectively. It can be seen from figures 11(a) and 11(b) that at sufficiently high values of the Froude number (above 2.6), the flexible-torso model captures the stride length and stride frequency of the horse more accurately than the rigid-torso model. For the case of the dog morphology, figures 11(c) and 11(d) indicate that the rigid-torso model takes longer strides at lower frequency compared to the animal data, while the introduction of torso flexibility results in more accurate predictions of the stride length and frequency for the available speeds, which are all above 2.26.

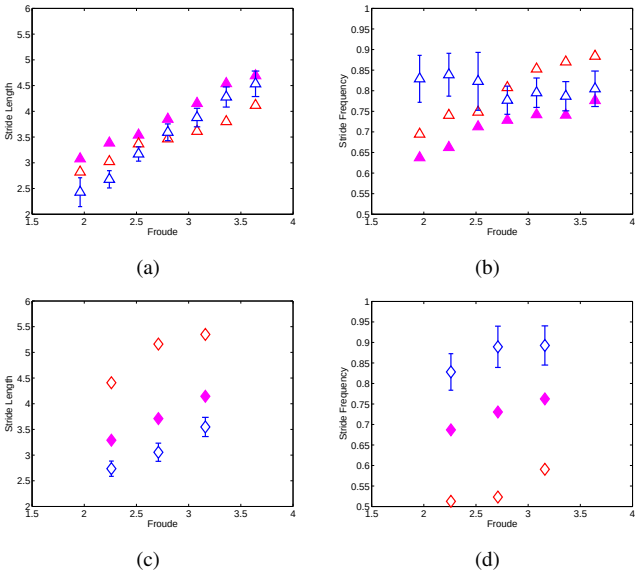

Fig. 11. The non-dimensional stride length and stride frequency of the energy efficient motions corresponding to the horse (a, b) and the dog (c, d) in figure 10. The animal data is represented by magenta filled symbols while the values predicted by the flexible torso and the values predicted by the rigid-torso are represented by blue and red symbols, respectively.

Generally, to maintain high speeds in the absence of torso flexibility, the rigid-torso model requires larger angular excursions of the legs relative to the torso (flatter touchdown and liftoff angles) and sufficient angular rates; see also figure 5. Clearly, this requirement increases the cost of transport due to the energy lost in hip actuators to sustain leg recirculation. On the other hand, the flexible-torso model requires smaller angular excursions relative to the torso to maintain these high speeds; for, in this case, leg recirculation is facilitated by the torso's flexion and extension oscillations. Given that torso oscillations are sustained by the non-ideal torso spring, which contributes less to the cost of transport than the non-ideal motors that supply the hip torques required for leg recirculation, the flexible-torso model requires less energy to maintain high speeds.

In summary, the results in figures 10 and 11 suggest that animals increasingly employ their torso at high speeds to avoid more pronounced leg motions that would otherwise be necessary to sustain such speeds. These leg motions would increase the energetic cost of transport due to the fact that, in the absence of torso flexion-extension oscillations, they would have to be realized primarily by the hip muscle units, the recruitment of which comes at a higher cost than that of elastic elements located in the animal's back – this issue is also

discussed in section VII-C below; see also figure 12. Hence, the flexible-torso model offers a more reliable predictive tool of quadrupedal animal running than the rigid-torso model.

It should be emphasized that the computation of the metabolic COT for *different* animals using the *same* reduced-order model is conducted in a direct manner; that is, without relying on empirical formulas and data fitting *specific* to an animal as in (Herr & McMahon, 2001; Herr et al., 2002), for example. In our case, the energy required to sustain the motion is calculated directly from the model by incorporating non-ideal torque sources and elastic elements, with efficiencies that are kept constant and equal to the biologically plausible values of muscle and tendon efficiency provided in section V-B. Given that estimating the metabolic COT from oxygen consumption measurements of running animals requires cumbersome experimental procedures, the proposed approach offers a simple way to predict, in a relatively reliable fashion, the energetic requirements of running for different quadrupedal animals running at different velocities.

Finally, note that the inertia properties of the leg with respect to the hip joint dramatically affect energy economy. As figure 10 shows, regardless of the value of the Froude number, the metabolic COT of the dog is much larger – nearly double – than that of the horse, despite the fact that the relative leg mass of the dog, $M_{\rm leg}$, is smaller than that of the horse. At first sight, this appears to contradict the results of figure 9, which shows that increasing the relative leg mass, $M_{\rm leg}$, increases the mechanical COT. The reason is that figure 9 was obtained by changing $M_{\rm leg}$ *only*, keeping the rest of the parameters constant. Clearly though, the horse and the dog models differ in other parameters, which significantly influence energy consumption. In particular, the (dimensionless) moment of inertia of the leg with respect to the hip joint $M_{\rm leg}d_{\rm leg}^2+I_{\rm leg}$ in the two models is significantly different: 0.05 for the horse and 0.08 for the dog, i.e., 1.6 times that for the horse. This discrepancy, not only in the value of the relative mass, but in the distribution of the leg's inertia about the hip join can explain the lower efficiency of the dog model considered relative to the horse.

To further explore the dependence of the metabolic COT on the inertia properties of the leg – not just the relative mass $M_{\rm leg}$ – consider a "test" flexible-torso model in which the dimensionless quantities $\{M_{\rm leg}, I_{\rm leg}, d_{\rm leg}\}$ characterizing the inertia properties of the leg obtain values equal to those of the dog model, while the rest of the parameters $\{I, d, \kappa_{\rm leg}, \kappa_{\rm tor}\}$ are kept equal to those of the horse model considered. The corresponding metabolic COT for this test model is depicted in figure 10 for $Fr \in \{2.24, 2.52, 2.80, 3.08\}$. It can be seen that, despite the great discrepancy between the test and the dog models, the corresponding values of the metabolic COT are very close. This implies that the inertia properties of the leg $\{M_{\rm leg}, I_{\rm leg}, d_{\rm leg}\}$ dominate the value of the metabolic COT. These observations indicate that a light-weight and small-inertia leg is crucial to energy economy, in agreement with (Ananthanarayanan et al., 2012; Seok et al., 2013).

C. Metabolic and mechanical COTs

To provide further intuition on how individual factors – i.e., the mechanics of the motion itself and the non-ideal actuators and springs used to sustain it – contribute to the computation of the metabolic COT, figure 12 presents the total metabolic COT and its components. The data shown in figure 12 are obtained based on the flexible- and rigid-torso models adapted to the dog and the horse morphologies, for values of the Froude number at which animal data are available.

The mechanical COT captures merely the cost of leg recirculation, assuming ideal torque generating and elastic energy storing elements. Clearly, at the Froude number values of figure 12 the mechanical COT is larger for the rigid-torso model implying that torso flexibility reduces the energy requirement. Notice, however, that as the Froude number decreases, the difference between the mechanical COT predicted by the rigid-torso and the flexible-torso models decreases as well; see figure 12(b) at $Fr = 1.96$ for example. This is consistent with the comparison in figure 4.

As figure 12 shows, when non-ideal hip actuators are considered the difference between the rigid-torso and the flexible-torso models is further amplified, particularly as the Froude number increases. This is clear from figure 12(b) and can be explained by the fact that leg recirculation in the rigid-torso model is realized predominantly through the hip actuators, which entail an energy cost that is higher compared to that of non-ideal springs in the torso. In fact, it is evident from figure 12 that the contribution of non-ideal springs to the metabolic COT is relatively smaller in size, implying that energy-efficient running can be achieved either by incorporating flexible elements in the torso to relief the hip actuators or by the design of highly-efficient actuators as in (Seok et al., 2013).

On a final note, a simple relation between the metabolic and the mechanical COT for a given periodic motion can be established. Under the assumption of a periodic motion, the energy supplied by the actuators doing positive work over a stride is equal to the energy lost in the actuators doing negative work plus the energy lost at the impacts with the ground during that stride, i.e.,

$$\int_0^T ([u_{\rm a}\dot{\varphi}_{\rm a}]^+ + [u_{\rm p}\dot{\varphi}_{\rm p}]^+)d\tau - \int_0^T ([u_{\rm a}\dot{\varphi}_{\rm a}]^- + [u_{\rm p}\dot{\varphi}_{\rm p}]^-)d\tau - |\Delta E_{\rm imp}| = 0,$$

where $\Delta E_{\rm imp}$ is the total energy lost at impacts over the stride. This implies,

$$\int_0^T ([u_{\rm a}\dot{\varphi}_{\rm a}]^- + [u_{\rm p}\dot{\varphi}_{\rm p}]^-)d\tau < \int_0^T ([u_{\rm a}\dot{\varphi}_{\rm a}]^+ + [u_{\rm p}\dot{\varphi}_{\rm p}]^+)d\tau,$$

and thus, the mechanical COT defined in (33) satisfies

$$c_{\rm mc} < \frac{1}{2(1+M_{\rm leg})TFr}\int_0^T 2([u_{\rm a}\dot{\varphi}_{\rm a}]^+ + [u_{\rm p}\dot{\varphi}_{\rm p}]^+)d\tau \ . \tag{38}$$

On the other hand, for the metabolic COT defined in (33), since $P_2, P_3 > 0$

$$\begin{aligned} c_{\rm mt} &> \frac{1}{2(1+M_{\rm leg})TFr}\int_0^T P_1 d\tau \\ &> \frac{1}{2(1+M_{\rm leg})TFr}\int_0^T \frac{1}{\eta_1}([u_{\rm a}\dot{\varphi}_{\rm a}]^+ + [u_{\rm p}\dot{\varphi}_{\rm p}]^+)d\tau \ , \end{aligned}$$

where (34) and the facts that $\eta_2 > 0$ and $([u_a\dot{\varphi}_a]^- + [u_p\dot{\varphi}_p]^-) > 0$ have been used. In view of (38), the last inequality results in the simple relation

$$c_{mt} > \frac{1}{2\eta_1} c_{mc} \ . \tag{39}$$

Note that for the case where the efficiency of performing positive work is $\eta_1 = 0.25$ as in section V-B, (39) takes the particularly simple form

$$c_{mt} > 2c_{mc} \ . \tag{40}$$

A closer look at figure 12 reveals that at a given speed the minimum metabolic COT of a model is always more than two times of the mechanical COT, confirming (40). Given that the mechanical COT cannot be easily obtained in experiments with animals (Alexander, 2005), (40) could be used to provide an upper bound of the mechanical COT on the basis of estimates of the metabolic COT using oxygen consumption measurements from running animals.

VIII. Conclusions

In this paper, the energetics of quadrupedal running on the basis of the cost of transport (COT) was studied in a template setting. Two reduced-order models, one with rigid (non-deformable) torso and one with flexible, unactuated torso were introduced. Both models feature non-trivial leg inertia intended to capture the energy cost of leg recirculation, and a simple controller that regulates leg placement during flight was proposed to produce cyclic bounding motions. By comparing the motions generated by the two models in terms of the mechanical COT it is deduced that torso flexibility offers an advantage in terms of energy economy when the Froude number exceeds a particular value. Interestingly, this value agrees with the one at which transitions from trotting to galloping are observed in animals with different morphological characteristics (Alexander, 1989). The enhancement of energy efficiency afforded by the flexible torso is due to the contribution of the torso's dorsoventral oscillations to leg recirculation, thereby confirming the hypothesis in Alexander et al. (1985). Additional model-predicted conclusions regarding the stride frequency and stride length and their relation to the running speed are consistent with biological observations that appeared in the relevant literature.

To gain further insight on the proposed models and their predictive ability in capturing the energetics of quadrupedal animal running, a procedure for estimating the metabolic COT was proposed. Non-ideal torque generating and compliant elements were incorporated in the model using biologically plausible efficiency values that correspond to those of tendons and muscles performing positive and negative work. Despite the simple structure of the model and the inaccuracy with which certain model parameters can be identified from animal data, it is remarkable that the metabolic COT predicted by the flexible-torso model is in good agreement with the COT estimated using oxygen consumption measurements of different quadrupedal running animals.

Given that the flexible-torso model provides relatively accurate predictions of the energetic COT of different animals – and it does so in a direct way, without the use of animal-specific parameter fitting procedures – the results in this paper offer a simple way to make predictions about energy consumption in running quadrupeds and to quantify the effect of inertia and stiffness properties on gait energetics.

Acknowledgments

The work is supported in part by NSF grants CMMI-1130372 and IIS-1350721, and ARL contract W911NF-12-1-0117. The authors would like to thank the anonymous reviewers for their valuable comments and suggestions.

References

Alexander, R. (1988). *Elastic Mechanisms in Animal Movement*. Cambridge: Cambridge University Press.

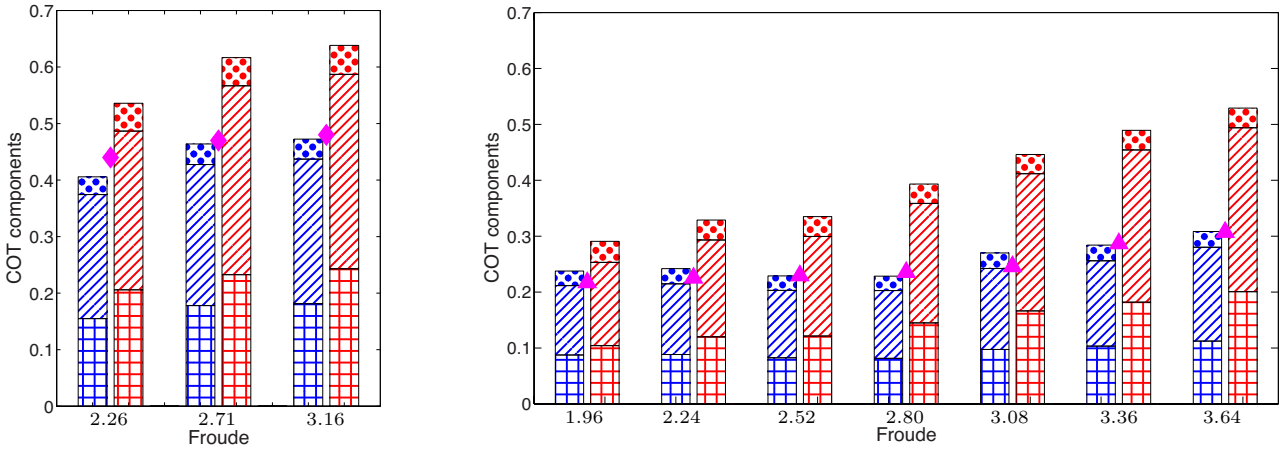

(a) Model adapted to the morphology of the dog.

(b) Model adapted to the morphology of the horse.

Fig. 12. The comparison of mechanical COT and metabolic COT for the flexible-torso (blue) and rigid-torso (red) models with the dog and horse physical parameters. The square pattern represents the mechanical COT. The diagonal pattern represents the increased value in COT when considering the efficiency of the actuators. The dot pattern represents the contribution of the non-ideal springs in the metabolic COT. The sum of these three component constitutes the metabolic COT shown in figure 10(a) and figure 10(b). The metabolic COT estimated based on animal data is represented by diamonds for the dog and by triangles for the horse, as in figure 10.

Alexander, R. (1989). Optimization and gaits in the locomotion of vertebrates. *Physiological Reviews*, *69*(4), 1199–1227.

Alexander, R. (2005). Models and the scaling of energy costs for locomotion. *Journal of Experimental Biology*, *208*(9), 1645–1652.

Alexander, R., Dimery, N., & Ker, R. (1985). Elastic structures in the back and their role in galloping in some mammals. *Journal of Zoology*, *207*(4), 467–482.

Amit, T., Gomberg, B., Milgram, J., & Shahar, R. (2009). Segmental inertial properties in dogs determined by magnetic resonance imaging. *The Veterinary Journal*, *182*(1), 94–99.

Ananthanarayanan, A., Azadi, M., & Kim, S. (2012). Towards a bio-inspired leg design for high-speed running. *Bioinspiration & Biomimetics*, *7*(4), 046005.

Blickhan, R. (1989). The spring-mass model for running and hopping. *Journal of Biomechanics*, *22*(11-12), 1217–1227.

Blickhan, R., & Full, R. J. (1993). Similarity in multi-legged locomotion: Bouncing like a monopode. *Journal of Comparative Physiology A*, *173*(5), 509–517.

Buchner, H., Savelberg, H., Schamhardt, H., & Barneveld, A. (1997). Inertial properties of Dutch Warmblood horses. *Journal of Biomechanics*, *30*(6), 653–658.

Cao, Q., & Poulakakis, I. (2012). Passive quadrupedal bounding with a segmented flexible torso. In *Proceedings of the IEEE/RSJ International Conference on Intelligent Robots and Systems* (pp. 2484–2489).

Cao, Q., & Poulakakis, I. (2013). Quadrupedal bounding with a segmented flexible torso: passive stability and feedback control. *Bioinspiration & Biomimetics*, *8*(4), 046007.

Cao, Q., & Poulakakis, I. (2014). On the energetics of quadrupedal bounding with and without torso compliance. In *Proceedings of the IEEE/RSJ International Conference on Intelligent Robots and Systems* (pp. 4901–4906).

Cao, Q., & Poulakakis, I. (2015). Control of quadrupedal bounding with flexible torso and speed transitions with sums of squares verification. In *International Symposium on Swarm Behavior and Bio-inspired Robotics (SWARM)*. Kyoto, Japan. (In review)

Collins, S. H., Ruina, A., Tedrake, R., & Wisse, M. (2005). Efficient bipedal robots based on passive-dynamic walkers. *Science*, *307*(5712), 1082–1085.

Culha, U., & Saranli, U. (2011). Quadrupedal bounding with an actuated spinal joint. In *Proceedings of the IEEE International Conference on Robotics and Automation* (pp. 1392–1397).

Deng, Q., Wang, S., Xu, W., Mo, J., & Liang, Q. (2012). Quasi passive bounding of a quadruped model with articulated spine. *Mechanism and Machine Theory*, *52*, 232–242.

Eaton, M. D., Evans, D. L., Hodgson, D. R., & Rose, R. J. (1995). Effect of treadmill incline and speed on metabolic rate during exercise in thoroughbred horses. *Journal of Applied Physiology*, *79*(3), 951–957.

Farley, C. T., Glasheen, J., & McMahon, T. A. (1993). Running springs: speed and animal size. *Journal of Experimental Biology*, *185*(1), 71–86.

Full, R., & Koditschek, D. E. (1999). Templates and anchors: Neuromechanical hypotheses of legged locomotion on land. *Journal of Experimental Biology*, *202*, 3325–3332.

Gabrielli, G., & von Karman, T. (1950). What price speed? specific power required for propulsion of vehicles. *Mechanical Engineering*, *72*(10), 775–781.

Guckenheimer, J., & Holmes, P. (1996). *Nonlinear Oscillations, Dynamical Systems, and Bifurcations of Vector Fields* (Vol. 42). New York: Springer-Verlag.

Haberland, M., Karssen, J. G. D., Kim, S., & Wisse, M. (2011). The effect of swing leg retraction on running energy efficiency. In *Proceedings of the IEEE/RSJ International Conference of Intelligent Robots and Systems* (pp. 3957–3962).

Haueisen, B. M. (2011). *Investigation of an Articulated Spine in a Quadruped Robotic System* (Unpublished doctoral dissertation). The University of Michigan.

Heglund, N. C., & Taylor, C. R. (1988). Speed, stride frequency and energy cost per stride: how do they change with body size and gait? *Journal of Experimental Biology*, *138*(1), 301-318.

Herr, H. M., Huang, G. T., & McMahon, T. A. (2002). A model of scale effects in mammalian quadrupedal running. *Journal of Experimental Biology*, *205*(7), 959–967.

Herr, H. M., & McMahon, T. A. (2001). A galloping horse model. *The International Journal of Robotics Research*, *20*(1), 26–37.

Hildebrand, M. (1961). Further studies on locomotion of the cheetah. *Journal of Mammalogy*, *42*(1), 84–91.

Hoyt, D. F., & Taylor, C. R. (1981). Gait and the energetics of locomotion in horses. *Nature*, *292*, 239 – 240.

Kram, R., & Taylor, C. R. (1990). Energetics of running: a new perspective. *Nature*, *346*(6281), 265–267.

Krasny, D. P., & Orin, D. E. (2004). Generating high-speed dynamic running gaits in a quadruped robot using an evolutionary search. *IEEE Transactions on Systems, Man, and Cybernetics, Part B: Cybernetics*, *34*(4), 1685–1696.

Maes, L. D., Herbin, M., Hackert, R., Bels, V. L., & Abourachid, A. (2008). Steady locomotion in dogs: temporal and associated spatial coordination patterns and the effect of speed. *Journal of Experimental Biology*, *211*(1), 138–149.

Margaria, R. (1976). *Biomechanics and Energetics of Muscular Exercise*. Oxford: Clarendon Press.

Marhefka, D., Orin, D., Schmiedeler, J., & Waldron, K. (2003). Intelligent control of quadrupedal gallops. *IEEE/ASME Transactions on Mechatronics*, *8*(4), 446–456.

McMahon, T. A., & Cheng, G. C. (1990). The mechanics of running: How does stiffness couple with speed? *Journal of Biomechanics*, *23*, 65–78. (Suppl. 1)

Miller, S., Van Der Burg, J., & Van Der Meche, F. (1975). Coordination of movements of the hindlimbs and forelimbs in different forms of locomotion in normal and decerebrate cats. *Brain Research*, *91*(2), 217–237.

Minetti, A., Ardigo, L., Reinach, E., & Saibene, F. (1999). The relationship between mechanical work and energy expenditure of locomotion in horses. *Journal of Experimental Biology*, *202*(17), 2329–2338.

Nanua, P. (1992). *Dynamics of a Galloping Quadruped* (Unpublished doctoral dissertation). Ohio State University.

Nanua, P., & Waldron, K. (1995). Energy comparison between trot, bound and gallop using a simple model. *Journal of Biomechanical Engineering*, *117*(4), 466-473.

Park, H.-W., & Kim, S. (2015). Quadrupedal galloping control for a wide range of speed via vertical impulse scaling. *Bioinspiration & Biomimetics*, *10*(2), 025003.

Pollock, C. M., & Shadwick, R. E. (1994). Relationship between body mass and biomechanical properties of limb tendons in adult mammals. *American Journal of Physiology*, *266*(3), 1016–1021.

Poulakakis, I. (2002). *On the passive dynamics of quadrupedal running* (Unpublished master's thesis). McGill University.

Poulakakis, I., Papadopoulos, E. G., & Buehler, M. (2006). On the stability of the passive dynamics of quadrupedal running with a bounding gait. *The International Journal of Robotics Research*, *25*(7), 669–687.

Poulakakis, I., Smith, J., & Buehler, M. (2005). Modeling and experiments of untethered quadrupedal running with a bounding gait: The Scout II robots. *The International Journal of Robotics Research*, *24*(4), 239–256.

Remy, C. D., Buffinton, K., & Siegwart, R. (2012). Comparison of cost functions for electrically driven running robots. In *Proceedings of IEEE International Conference on Robotics and Automation* (pp. 2343–2350).

Remy, C. D., Buffinton, K., & Siegwart, R. Y. (2010). Energetics of passivity based running with high-compliance series elastic actuation. In *Proceedings of Mechatronics Forum Biennial International Conference.*

Schmiedeler, J. P., & Funke, L. (2013). Unfinished business: Impulsive models of quadrupedal running gaits. In *Advances in Mechanisms, Robotics and Design Education and Research* (pp. 295–304). Springer.

Schmiedeler, J. P., Siston, R., & Waldron, K. J. (2002). The significance of leg mass in modeling quadrupedal running gaits. In G. Bianchi, J. C. Guinot, & C. Rzymkowski (Eds.), *ROMANSY 14: Theory and Practice of Robots and Manipulators* (pp. 481–488). Vienna: Springer.

Seipel, J. E. (2011). Analytic-holistic two-segment model of quadruped back-bending in the sagittal plane. In *Proceedings of ASME Mechanisms and Robotics Conference* (Vol. 6, pp. 855–861).

Seok, S., Wang, A., Chuah, M. Y., Otten, D., Lang, J., & Kim, S. (2013). Design principles for highly efficient quadrupeds and implementation on the MIT Cheetah robots. In *Proceedings of IEEE International Conference on Robotics and Automation* (pp. 3307–3312).

Seyfarth, A., Geyer, H., & Herr, H. (2003). Swing leg retraction: A simple control model for stable running. *Journal of Experimental Biology*, *206*, 2547–2555.

Smith, A., Poulakakis, I., Trentini, M., & Sharf, I. (2010). Bounding with active wheels and liftoff angle velocity adjustment. *The International Journal of Robotics Research*, *29*(4), 414-427.

Spong, M. W., Hutchinson, S., & Vidyasagar, M. (2005). *Robot Modeling and Control*. New York: Wiley.

Srinivasan, M. (2011). Fifteen observations on the structure of energy-minimizing gaits in many simple biped models. *Journal of The Royal Society Interface*, *8*(54), 74–98.

Srinivasan, M., & Ruina, A. (2005). Computer optimization of a minimal biped model discovers walking and running. *Nature*, *439*(7072), 72–75.

Taylor, C. R., Shkolnik, A., Dmiel, R., Baharav, D., & Borut, A. (1974). Running in cheetahs, gazelles, and goats: energy cost and limb configuration. *American Journal of Physiology*, *227*(4), 848–850.

Tedrake, R., Manchester, I. R., Tobenkin, M., & Roberts, J. W. (2010). Lqr-trees: Feedback motion planning via sums-of-squares verification. *The International Journal of Robotics Research*, *29*(8), 1038–1052.

Tucker, V. A. (1975). The energetic cost of moving about. *American Scientist*, *63*(4), 413–419.

Westervelt, E. R., Grizzle, J. W., Chevallereau, C., Choi, J. H., & Morris, B. (2007). *Feedback Control of Dynamic Bipedal Robot Locomotion*. Taylor & Francis/CRC Press.

Yamasaki, R., Ambe, Y., Aoi, S., & Matsuno, F. (2013). Quadrupedal bounding with spring-damper body joint. In *Proceedings of IEEE/RSJ International Conference on Intelligent Robots and Systems* (pp. 2345–2350).

Zhang, Z. G., Fukuoka, Y., & Kimura, H. (2005). Stable quadrupedal running based on a spring-loaded two-segment legged models. In *Proceedings of the IEEE International Conference on Robotics and Automation* (Vol. 3, pp. 2601–2606).

Zou, H., & Schmiedeler, J. P. (2006). The effect of asymmetrical body-mass distribution on the stability and dynamics of quadruped bounding. *IEEE Transactions on Robotics*, *22*(4), 711–723.